Solar radiative output and its variability: Evidence and mechanisms

Article *in* Astronomy and Astrophysics Review · December 2004

DOI: 10.1007/s00159-004-0024-1

CITATIONS
343

READS
1,037

2 authors:

Claus Fröhlich
Arts &Science
222 PUBLICATIONS **7,381** CITATIONS
SEE PROFILE

Judith Lean
United States Naval Research Laboratory
128 PUBLICATIONS **11,983** CITATIONS
SEE PROFILE

The Astron Astrophys Rev (2004) 12: 273–320
Digital Object Identifier (DOI) 10.1007/s00159-004-0024-1

THE
ASTRONOMY
AND
ASTROPHYSICS
REVIEW

Solar radiative output and its variability: evidence and mechanisms

Claus Fröhlich[1], **Judith Lean**[2]

[1] Physikalisch-Meteorologisches Observatorium Davos, World Radiation Center, 7260 Davos Dorf, Switzerland
[2] E.O. Hulburt Center for Space Research, Naval Research Laboratory, Washington, DC 20375-5320, USA

Received 26 August 2004 / Published online 16 November 2004 –

Abstract. Electromagnetic radiation from the Sun is Earth's primary energy source. Space-based radiometric measurements in the past two decades have begun to establish the nature, magnitude and origins of its variability. An 11-year cycle with peak-to-peak amplitude of order 0.1 % is now well established in recent total solar irradiance observations, as are larger variations of order 0.2 % associated with the Sun's 27-day rotation period. The ultraviolet, visible and infrared spectral regions all participate in these variations, with larger changes at shorter wavelengths. Linkages of solar radiative output variations with solar magnetism are clearly identified. Active regions alter the local radiance, and their wavelength-dependent contrasts relative to the quiet Sun control the relative spectrum of irradiance variability. Solar radiative output also responds to sub-surface convection and to eruptive events on the Sun. On the shortest time scales, total irradiance exhibits five minute fluctuations of amplitude $\approx$ 0.003 %, and can increase to as much as 0.015 % during the very largest solar flares. Unknown is whether multi-decadal changes in solar activity produce longer-term irradiance variations larger than observed thus far in the contemporary epoch. Empirical associations with solar activity proxies suggest reduced total solar irradiance during the anomalously low activity in the seventeenth century Maunder Minimum relative to the present. Uncertainties in understanding the physical relationships between direct magnetic modulation of solar radiative output and heliospheric modulation of cosmogenic proxies preclude definitive historical irradiance estimates, as yet.

Key words: Sun: irradiance, activity, UV radiation, solar-terrestrial relations

Correspondence to: cfrohlich@pmodwrc.ch

1. Introduction

The radiative output of the Sun was termed the 'solar constant' until relatively recently when solar monitoring by satellite experiments revealed that it varies continuously. Commencing with the NIMBUS-7 spacecraft in the late nineteen seventies, the record of solar radiative output now extends without interruption to the present time, and exhibits variations on all time scales – from minutes to decades – accessed thus far.

Prior to the advent of space-based observations, astronomers and solar physicists argued that the radiative output of the Sun as a star changed in a substantial way only on evolutionary time scales, and was invariant for all practical purposes such as contemporary terrestrial effects. While it was recognized that the occurrence of sunspots might change the irradiance at the Earth, their effect was considered negligible because they cover at most a few tenths of a percent of the visible solar disk. As well, the results of a half-century of ground-based measurements of the 'solar constant' by the Smithsonian Institution were inconclusive, and likely reflected the influence of solar activity related variations on the terrestrial atmosphere.

Solar observations made with radiometers in space provided the first unequivocal evidence of solar irradiance variability on time scales from minutes to days and months [144]. The radiometers detected fluctuations that sometimes reached a few tenths of a percent and were associated with the movement of sunspots across the face of the solar disk visible at Earth as the Sun rotated on its axis. Establishing the reality of 11-year cycle-related solar irradiance variations proved more difficult. An overall decrease of the irradiance from the solar activity maximum in 1980 to activity minimum in 1986 was recognized as being of solar origin (rather than instrumental drift) only after the irradiance increased again towards the next solar maximum.

Scientific scepticism about the reality of solar radiative output variations, especially on solar-cycle time-scales, derived from the assumption that measurements made with absolute uncertainties of order ± 0.3 % precluded the unambiguous detection of true solar variability which a re-analysis of the Smithsonian observations [33, 36] had determined to be of smaller magnitude. But because of their high precision (0.001 % or better) the space-based radiometric measurements demonstrated that most, if not all, of the observed variability was indeed of solar origin. Since then, continuous variations in solar irradiance have been recorded on time scales from minutes, arising from p-mode oscillations and large flares, to the 11-year activity cycle, arising from changing solar activity. The important role of sunspots as a cause of radiative output variability has been quantified, additional bright sources of variability have been identified and speculated, and the spectral nature of the changes estimated. The extent of longer-term, inter-cycle radiative output changes during past centuries has also been speculated, based on cosmogenic isotope archives of solar activity and variations in sun-like stars. However, the record of direct irradiance observations ($\approx$ 25 years) is too short, as yet, to clarify the extent of the changes postulated.

1.1. Definition of solar radiative output

Irradiance, S, is the quantity that a solar radiometer observes at the annual mean sun-earth distance of one astronomical unit, $R = 1$ AU. It is the power of the Sun's electromag-

netic radiation received per unit area at the radiometer's entrance aperture, either in a given wavelength interval $d\lambda$ at λ, as *spectral* irradiance $F(\lambda)$, or integrated over all wavelengths as *total* irradiance, $S = \int F(\lambda)d\lambda$. This integral, which is the Sun's total radiative output in the direction to Earth, is the quantity referred to as the 'solar constant' for more than a century. Radiometers in the vicinity of the Earth can only record the power radiated from the solar hemisphere projected towards Earth. The power that the Sun radiates from its entire surface, called the solar luminosity, $L_\odot = 4\pi R^2 S$, has not been observed directly. This would require, for example, measurements made by a large number of space-based radiometers evenly distributed around the Sun.

Solar irradiance is composed of the radiance $I(\lambda)$ emitted from all elements of the solar hemisphere visible to the radiometer according to

$$F(\lambda) = \int_{\Omega_\odot} I(\lambda)d\Omega \tag{1}$$

where $\Omega_\odot$ is the solid angle that the solar disk extends at Earth for a given wavelength. Explicitly,

$$F(\lambda) = I_0(\lambda)\left(\frac{R_\odot}{R}\right)^2 2\pi \int_0^1 f(\mu, \lambda)\mu d\mu \tag{2}$$

where I_0 is the radiance at the disk center, $R_\odot$ is the radius of the Sun at a given wavelength, R the distance from the Sun to the radiometer, and $f(\mu, \lambda)$ is the center-to-limb radiance variation function with $\mu = \cos\theta$ for θ the angle subtended by the emitting surface element from the center of the solar disk. The center-to-limb function $f(\mu, \lambda)$ describes radiance variation across the disk which is mainly due to changes in the path length through the solar atmosphere, but also due to the variation of the angular variation of the radiance.

As the Sun's rotation axis is currently inclined by about 7° relative to the ecliptic plane the physical coordinates on the visible solar disk (heliospheric latitude of the center of the disk and the direction of the rotation axis) vary over the course of the year, from the perspective at Earth. With an ascending node around 5th June, the largest inclination with the solar south pole visible is in early March and with the north pole in early September. Thus, a persistent north-south radiance asymmetry such as may arise from different strengths of the activity in the two solar hemispheres, could produce an irradiance modulation with a one-year period.

1.2. Historical investigations of solar activity and radiative output variability

Although direct observations of the Sun's radiative output from space with high radiometric accuracy commenced only in 1978, telescopic observations of the Sun began in 1610 and led to the discovery of sunspots. Solar variability was established when the 11-year sunspot cycle was reported in 1843. Sunspot numbers have been recorded ever since, and reconstructed back to the time of the first observations [61]. Most extensive are the Greenwich Observatory records of sunspots (and also faculae) from 1882 to 1976. As Fig. 1 shows, sunspots provide a record of solar activity that now extends for almost four centuries, documenting large fluctuations in the amplitude of the 11-year cycle (Fig. 1b), and attendant phase changes as well (Fig. 1c).

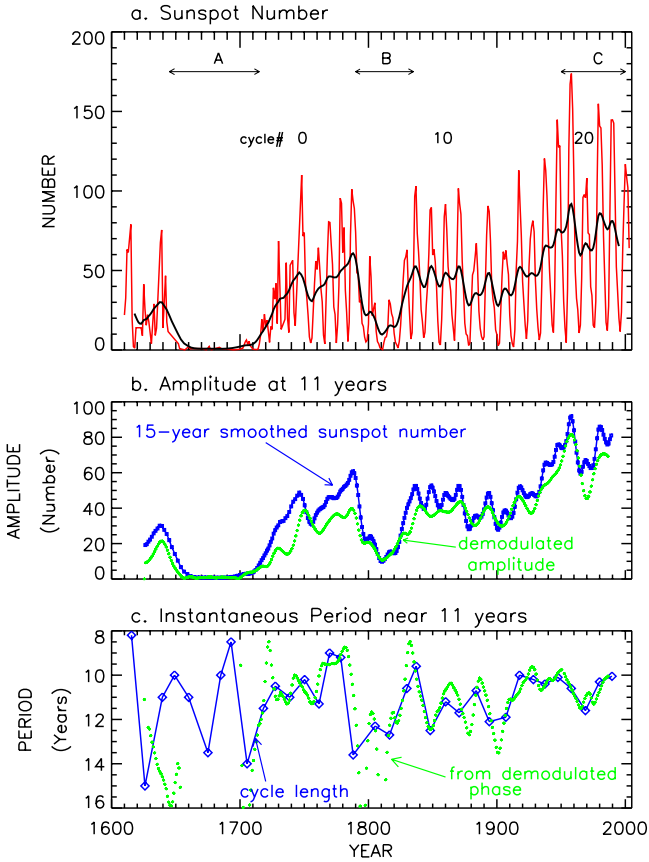

Fig. 1. Shown in **(a)** are variations in the annual mean group sunspot number, R_g, and in **(b)** and **(c)** the amplitude and phase of the 11-year cycle, during the past four hundred years. Amplitude and phase in **(b)** and **(c)** are determined from demodulation of the time series at a period of the solar cycle. The epochs A, B and C designate the Maunder Minimum, Dalton Minimum and Modern Maximum, respectively

Radiative output – brightness – changes were speculated to occur as a result of solar activity revealed by the sunspot record. Measurements were devised to detect changes in solar irradiance, culminating in the Smithsonian Astrophysical Observatory ground-based program from 1902 to 1957. Changes associated with the Sun's activity cycle were inferred for both the short-term decrease due to sunspots [2] and the 11-year cycle, shown as a positive correlation between sunspot numbers and the solar constant especially during the strong solar cycle 19 [1,3]. However, the determined amplitudes were nearly an order of magnitude higher than evident in the subsequent space-based record: the measurements failed to unambiguously detect real changes because of interference by the Earth's atmosphere. As a result, the view that the total radiative output was a constant quantity prevailed until the 1980s, when space-based records became available. (Hufbauer [62] and Hoyt and Schatten [59] provide historical details)

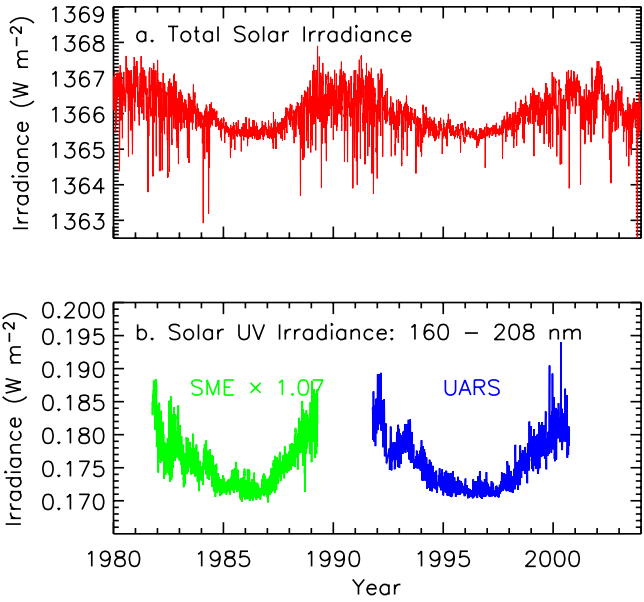

Fig. 2. Variation of the daily mean **(a)** total and **(b)** spectral (160–208 nm) solar irradiance during the last 25 years. The total irradiance record is a composite of observations from multiple spacecraft (PMOD composite). The two primary UV data sets are from the Solar Mesosphere Explorer (SME) and the Upper Atmosphere Research Satellite (UARS)

1.3. Knowledge of contemporary radiative output variability

From measurements made during the last 25 years by accurate radiometers in space, solar electromagnetic radiation is now understood to vary at all wavelengths, and on all time scales (e.g., [73]). The spectral irradiance variations $F(\lambda)$ produce a net change of order 0.1 % in total radiative output, S, during recent 11-year cycles, on which are superimposed larger variations of a few tenths of a percent on shorter time scales. Figure 2 shows plots of daily mean values of the total and UV spectral irradiance time series now available. Spectral irradiance, shown in Fig. 3, and the amplitude of the spectrum variability are both strongly wavelength dependent. In general, the visible, near UV and near IR spectral regions, where the flux of the Sun's electromagnetic radiation peaks, vary the least – by a few tenths of a percent during the 11-year activity cycle. Significantly more variable is solar radiation at wavelengths both shorter and longer than the peak of the curve – in the ultraviolet (Fig. 2b), X-ray and radio portions of the electromagnetic spectrum.

Knowledge of solar spectral irradiance variability is poor except at wavelengths shorter than visible/near UV and longer than IR. This is because relatively reliable long term observations have been possible only at wavelengths for which irradiance variability exceeds a few percent. The percentage level variations of UV radiation emergent from the Sun's upper photosphere in the band from 160 nm (originating near the temperature minimum regions) to 208 nm (the Al ionization edge) can be seen in Fig. 2b to vary by an order of magnitude more than the total irradiance (Fig. 2a) which emerges from

lower photospheric layers. Evident in the UV spectrum, as for total irradiance, are variations associated with the 27-day solar rotation, monthly to annual fluctuations, and the prominent 11-year cycle. Unlike the total irradiance for which an uninterrupted record exists since 1978, the UV spectral irradiance record is intermittent in this interval.

1.4. Relevance for models of the sun

The Sun and its variability provide unique constraints on models of stellar evolution, which in turn provide scenarios for solar variability on exceedingly long time scales, not accessible by irradiance observations. Luminosity, radius and age, fundamental parameters in standard models of stellar evolution, are known relatively accurately for the Sun, although the transfer of irradiance values to luminosity is complicated. However, stellar evolution models have only very simple atmospheres that lack the dynamo-driven magnetic fields that produce activity in the Sun, so accommodating irradiance cycles is problematic. Furthermore, a luminosity averaged over several 1000 years is more appropriate than a value determined from contemporary observations but this requires knowledge of long-term solar irradiance changes. Even if the transfer from irradiance to luminosity could be performed accurately, and a long-term average determined, the uncertainty in irradiance simulated by these models would be no better than about 0.1 % which cannot adequately constrain solar models. Knowledge of the Sun's radius can potentially calibrate solar models but changes in the optically observed value, which is normally used, are not known (for a review see, e.g., [107]). Thus far, solar evolution theory only provides evidence for radiative output changes over very long time scales, such as the increase of the luminosity during the last three billion years by about 30 % (e.g., [116]). The standard values used to calibrate current models are: radius $R_\odot = 6.9599 \cdot 10^8$m, luminosity $L_\odot = 3.846 \cdot 10^{26}$W (corresponding to a 'solar constant' of 1367.6 W m^{-2}), age $t_\odot = 4.65$ Gy, and a photospheric metallicity $Z/X = 0.0245$.

Standard models of the Sun itself (see, e.g., [105]) incorporate more physical parameters (opacities and equation of state) and include processes such as microscopic diffusion, penetrative convection and mass loss. At present helioseismology affords the most important constraints for standard solar models, by allowing comparison with a 'seismic' model, inverted from observed, highly accurate p-mode frequencies (see, e.g., [130]). New helioseismic results have substantially improved our knowledge of the internal structure and dynamics of the Sun. The deficit of the observed neutrinos, for example, is no longer a problem of understanding stellar evolution, but rather one of the behaviour of the neutrinos. Helioseismology also provides some evidence for solar-cycle related changes at the base of the convection zone, within it and below the surface which may be related to structural changes (see, e.g., [5, 12, 56]). Changes of the Sun's radius would be a further indication of structural changes, for which the ratio $W = (dL/L)/(dR/R)$ provides important information about the location of the perturbation within the Sun leading to such variations. Determination of W and of possible changes over the solar cycle is the aim of PICARD to be launched in 2008 [129].

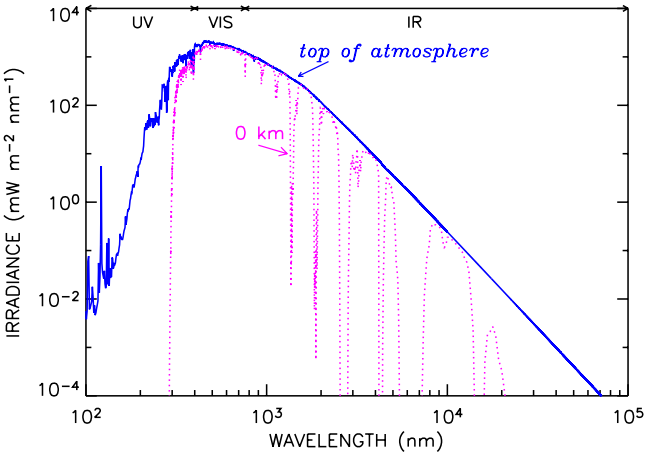

Fig. 3. Shown are the Sun's spectral irradiance at the top of the Earth's atmosphere and at the Earth's surface (0 km). Gases in the Earth's atmosphere absorb solar radiation, especially in the UV and IR spectrum (e.g., O_2, O_3, H_2O, CO_2)

1.5. Relevance for global change on earth

A balance between incoming solar radiation (which peaks in the visible spectrum, Fig. 3), referred to as 'short-wave', and outgoing terrestrial radiation (which peaks in the vicinity of 10 μm), referred to as 'long-wave', establishes the equilibrium temperature in the vicinity of the Earth's surface. The spectrum of the Sun's irradiance at the top of the Earth's atmosphere is therefore a critical determinant of Earth's climate (e.g., [100]). Both the solar spectral irradiance variability and the processes that facilitate climate response to solar radiative forcing are strongly wavelength dependent. There is considerable atmospheric absorption in the ultraviolet (UV) and near infrared (IR) spectral regions, which depletes certain spectral regions and produces a solar irradiance spectrum at the Earth's surface (0 km in Fig. 3) that differs substantially from the unattenuated spectrum.

Since the Sun's electromagnetic radiation is the primary source of energy for the Earth, even small variations in irradiance have the potential to influence Earth's climate and atmosphere, including the ozone layer (e.g., [22, 50, 76, 110]). Furthermore, the extinction of solar radiation by absorption and scattering in the Earth's atmosphere, and its reflection by land surfaces and oceans are strongly wavelength dependent, as are the processes through which climate responds to radiative input changes, involving atmospheric constituents such as water vapour and ozone, surface properties such as sea ice and snow cover, and most importantly clouds (e.g., [93]). Reliable knowledge of solar-induced variations is essential for understanding and attribution of anthropogenic influences on Earth's climate [126] and changes of the ozone layer in the stratosphere (e.g., [47]). This requires the specification of solar spectral irradiance from 0.1 to 100 micron on time scales of years to centuries.

Climate model simulations of Earth's surface temperature response to solar variability in past centuries require as input estimates of historical irradiance. However, on climatological and solar-evolution time scales the irradiance database acquired thus

far is extremely short. This has motivated the development of variability models that reconstruct past irradiance changes, based on understanding the sources of variability evident in the contemporary database and their relationship to solar activity indices. Most models adopt a speculated (but unproven) long-term component which produces an irradiance increase in the range 0.2 to 0.4 % from the Maunder Minimum to the present maxima (e.g., [28, 58, 74, 87]). In response to such irradiance reconstructions, simulations of climate change in recent centuries suggest solar-related surface temperature changes between 0.2 K [21] and 0.4 K [111, 112], which are unable to account for global warming in the past few decades.

The state of the terrestrial upper atmosphere and ionosphere depends crucially on solar irradiance in the extreme ultraviolet spectrum, which varies significantly – by factors of two to an order of magnitude during the solar cycle. These irradiance changes at short wavelengths produce dramatic modulation of temperature and densities of the upper atmosphere (e.g., [73]). But since the contribution to the total radiative output of solar irradiance variations at wavelengths shorter than Ly-α is negligible, this spectral region is not considered here.

2. Properties of solar radiation

The Sun emits radiation primarily from the vicinity of its surface. Some 99 % of solar radiative output – that at wavelengths from 275 to 4900 nm – emerges from the photosphere. As Fig. 4 shows, the brightness temperature of the quiet Sun's surface is 6520 K decreasing to about 4400 K at the top of the photosphere after which the temperature decline with height reverses into the overlying chromosphere. Height is defined here as the radial distance above unit optical depth in the continuum at 500 nm, $\tau_{500} = 1$. Above the chromosphere, in the transition region and the corona, the temperature increases to a few million degrees as the outer solar atmosphere expands into the heliosphere. Here, the intensity of the emergent high energy (short wavelength) radiation is very weak and contributes only a few $\mathrm{mW\,m^{-2}}$ to the Sun's total radiative output of $\approx 1365\ \mathrm{W\,m^{-2}}$.

2.1. Spectral distribution

Although the spectrum of photospheric radiation appears as a relatively smooth continuum when viewed with moderate spectral resolution, as in Fig. 3, it actually comprises numerous spectral features shown in Fig. 5. Absorption and emission processes of gases in the Sun's atmosphere – H, He, C, N, O, Mg, Al, Si, Ca and Fe in various states of ionization – produce spectral features with widths typically a few tens of pm. Many spectral features are attributable to hydrogen, the most common component of the Sun's atmosphere, including prominent emission and absorption lines (e.g., at 121 nm and 656.3 nm, respectively). Likewise, the second most common solar atmosphere constituent, He, produces strong line emission (e.g., at 30.4 nm and 58.4 nm) and absorption (e.g., at 1083 nm).

In addition to composition, temperature in the solar atmosphere is a primary determinant of solar spectrum structure. In fact, in the photosphere (heights less than $\approx$ 525 km)

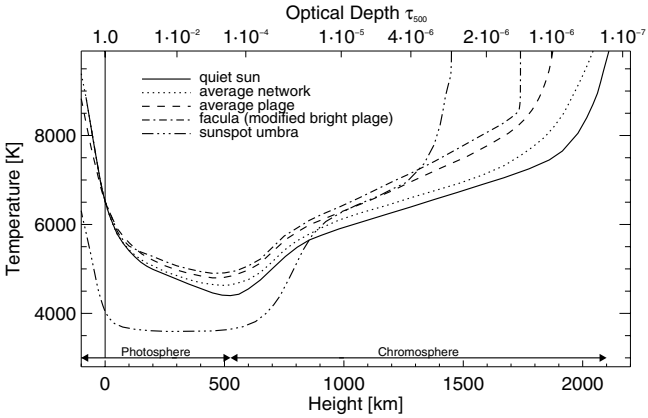

Fig. 4. Shown are temperature distributions in the solar atmosphere for the quiet Sun and different magnetic features, adapted from [29] and [124]. The density of the atmosphere varies as $\rho = 2.77 \cdot 10^{-4}, 4.87 \cdot 10^{-6}, 1.71 \cdot 10^{-10}\ \mathrm{kg\,m^{-3}}$ for $h = 0, 525, 2100$ km, respectively

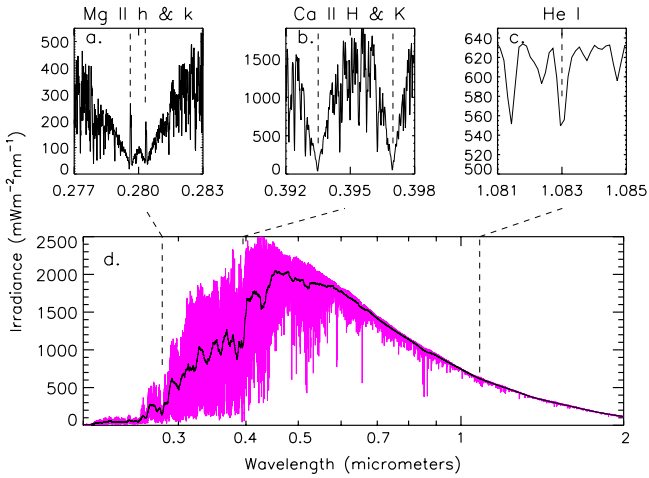

Fig. 5. The spectral distribution of the solar irradiance is shown at high resolution for isolated spectral regions corresponding to **(a)** the Mg h and k, **(b)** the CaII H and K Fraunhofer lines, and **(c)** the He I absorption line. In **(d)** a theoretical spectrum is shown at all wavelengths [69]

and in the chromosphere (heights from $\approx$ 525 km to $\approx$ 2100 km) measurements of radiation spectrum intensities are used to infer the solar atmospheric temperature distribution by adjusting the spectrum from radiative transfer calculations to agree with the spatially averaged spectrum of the quiet Sun. The quiet solar spectrum (see, e.g., [7]) has a maximum brightness temperature of about 7500 K at 1.6 µm where the solar atmosphere has minimum opacity (the H^- bound-free opacity is zero at this wavelength) and the deepest photospheric layers (≈ -40 km) are accessible as shown in Fig. 6. From this minimum, opacity increases towards shorter wavelengths due to H^- bound-free absorption and the Balmer, Al, Si and Lyman edges. Longward, opacity increases due to H^- free-free absorption. As opacity increases, the brightness temperature decreases because increas-

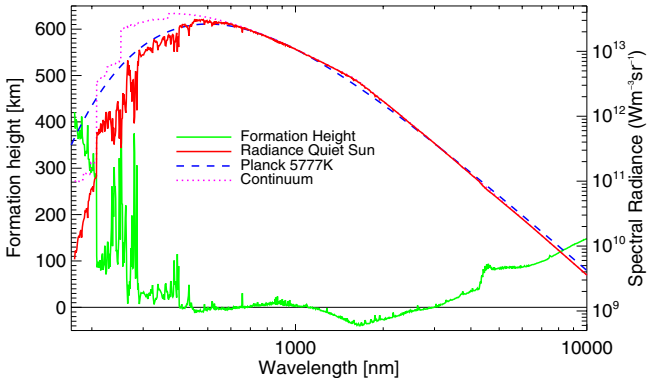

Fig. 6. Shown by the green line is the height of formation of the Sun's radiation at different wavelengths, together with the spectral radiance of a quiet Sun (red), the spectrum of a black body radiation at 5777 K (blue dashed), and the spectral radiance of the continuum (red dotted)

ingly higher layers of the photosphere have lower temperatures. The resulting spectrum is called a continuum because it does not contain any lines (see 'Continuum' in Fig. 6). For the quiet Sun a minimum value of about 4450 K is reached at around 150 μm and near 160 nm. At wavelengths $\lambda > 150$ μm and $\lambda < 160$ nm the brightness temperature increases and the lines in the spectrum are seen in emission rather than absorption. The intensity of the lines are related to the temperature distribution via the formation height of the line (see 'Formation Height' in Fig. 6).

Radiative transfer models are able to match not only the general properties of the solar spectrum, but also the observed emission near the centers of the Ca II and Mg II lines (Fig. 5) by including non-LTE calculations above the temperature minimum with temperature distributions such as those shown in Fig. 4 (e.g., [29, and references therein]). These atmospheric models are *semi-empirical,* because the temperature is adapted to reproduce the observed spectral intensities; the law of conservation of energy is *not* used. Transport of the energy in the chromosphere and corona is not by radiation only, but includes other mechanisms which are not understood sufficiently to be modelled adequately.

2.2. Spatial distribution

Solar radiation is not distributed homogeneously on the disk of the Sun viewed from the Earth. The radiance from a spatial element of the solar atmosphere varies from the center of the Sun's disk to the limb, in different ways at different wavelengths. Superimposed on this center-to-limb variation is a changing distribution of bright and dark emission associated with various solar features, such as sunspots, faculae and network. The solar images in Fig. 7 illustrate the distinct character of active regions in different solar atmospheric regimes and their associations with photospheric magnetic flux. Compact, bright faculae tend to occur in the vicinity of large sunspots, both of which signify regions of enhanced magnetic flux. The magnetic fields in these features alter the temperature and density of the solar atmosphere, and thereby the emitted radiation, in

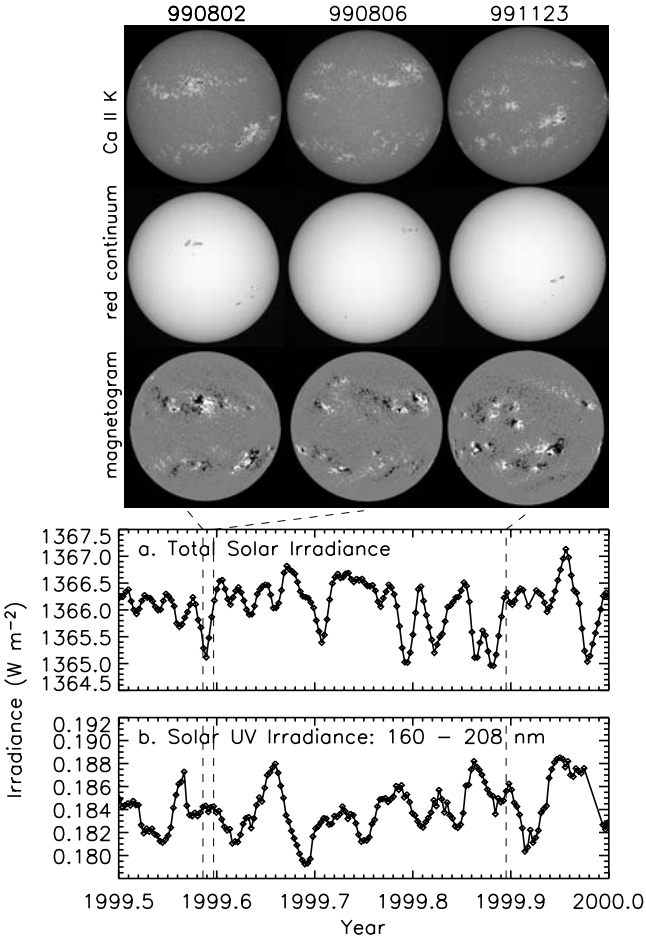

Fig. 7. Images of the Sun recorded by the Photometric Solar Precision Telescope (PSPT) in the UV Ca K line and the red continuum are compared with magnetograms from the U.S. National Solar Observatory (NSO). Changes in **(a)** total and **(b)** UV solar irradiance (from Fig. 2) are traceable to changes in magnetic features

wavelength-dependent ways. Compact, dark sunspots are the primary magnetic signature in visible and red continuum photospheric images, such as those in Fig. 7. Here the photospheric gas pressure is large enough to balance the magnetic field strength. Higher, in the solar chromosphere, the dominant magnetic features are extended, bright plages, in which magnetic fluxes are smaller than in sunspots. These features are evident in the Ca K images in Fig. 7.

Temperature distributions for typical activity-related features are shown in Fig. 4. Compared with the quiet Sun are average network, average plage, facula or bright plage, and sunspot umbra. Sunspots are darker and cooler than the surrounding photosphere at all wavelengths except possibly at the shortest EUV wavelengths [96]. Faculae and plages are generally brighter except possibly at the center of the disk and in the near

IR [30, 72, 95]. When active features are present in the solar atmosphere, their different temperature distributions and altered radiance change the solar spectrum by an amount proportional to their fractional coverage of the solar surface. Thus the continual eruption, evolution and submergence of magnetic field produces time-dependent temperature and thus radiance inhomogeneities, which subsequently alter solar irradiance. For example, the irradiance time series in Fig. 7 illustrate the decrease in total solar irradiance, but not in UV irradiance, coincident with a large sunspot group present near the central meridian shown in the left column of the images of Fig. 7.

2.3. Solar radiation proxies

Different regions of the solar spectrum arise from radiation formed in different solar atmospheric layers. Since magnetic fields produce different conditions of temperature and density in different atmospheric layers, observing the Sun at selected wavelengths or wavelength regions formed over a range of different temperatures provides a tool for detecting and quantifying the impact of solar activity throughout the solar atmosphere, and hence on the emergent radiation at many wavelengths. Particularly useful in this regard are solar emission and absorption line features in which the cores of the lines form above the temperature minimum region (i.e., in the chromosphere). This is the case for the Mg II and Ca II doublets and the He I line shown in the top panels in Fig. 5. When measured as an average over the disk (sun-as-a-star observation), ratios of the core emission relative to the wings of such spectral features yield information about the prevailing global temperature structure pertaining to an area-weighted average of the distributions from specific magnetic features. Quantitative relationships exist among various globally integrated fluxes as a result of the significant spatial correlations of their variability sources, although the spatial scales are altered by the different pressure conditions. In this way, photospheric faculae are identified in addition to plage and enhanced network from indices in the upper photosphere and chromosphere.

Figure 8 compares the variations in three different indices of solar activity that have been widely used to infer irradiance variations. The Mg II chromospheric index is the core-to-wing ratio of the Mg II doublet (at 280 nm), shown in Fig. 5a. This index tracks closely the flux variations in the equivalent width of the He I line at 1083 nm and the core of the Ca II K emission at 393 nm (also shown in Fig. 5). Compared in Fig. 8 with the chromospheric Mg II index are the 10.7 cm radio flux, whose fluctuations reflect a combination of chromospheric (longer term) and coronal (short term) influences, and the sunspot number, which is a visually determined, numerical rather than physical index, but the longest available direct indicator of solar activity (Fig. 1).

3. Observational evidence for irradiance variability

3.1. Radiometric measurements of total irradiance from space

A first attempt to use electrically calibrated radiometers (ECRs) in space was made on the Mariner VI and VII missions to Mars in 1969 [102, 103] in order to test spacecraft

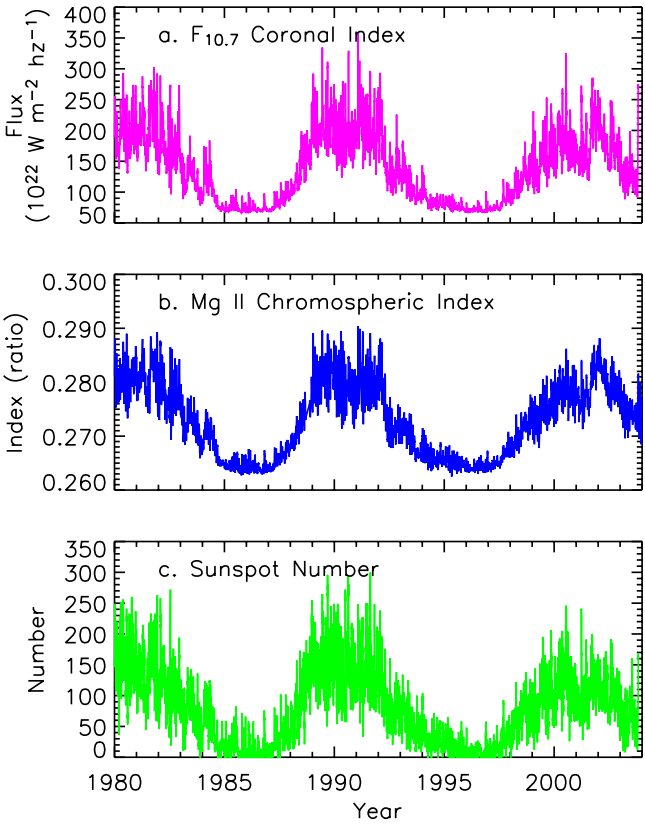

Fig. 8. Shown are the time variations of daily values of three solar activity proxies that have been used in various ways to infer solar irradiance variations. The radio flux at 10.7 cm ($F_{10.7}$) in **(a)** is available since 1947, and primarily reflects brightness changes in the corona, whereas the Mg II index of chromospheric activity in **(b)** is available only since 1978 and closely simulates changes in global brightness associated with faculae and plages. The sunspot number in c) is a generic indicator of solar activity, available since 1610, as shown in Fig. 1

behaviour under extended exposure to solar radiation. However, the results were unable to distinguish instrumental effects from true solar variability at the few tenths of a percent level (see also [37]). Conclusive evidence for solar irradiance variability was achieved only after ECRs were launched on space platforms to monitor the Sun more or less continuously, that is with the launch of the Earth Radiation Budget experiment on NIMBUS 7 in November 1978. In early 1980 the Solar Maximum Mission satellite (SMM) followed, then the Earth Radiation Budget Experiment (ERBE), the Upper Atmosphere Research Satellite (UARS), the European Retrievable Carrier (EURECA), the Solar and Heliospheric Observatory (SOHO), ACRIMSAT and most recently the Solar Radiation and Climate Experiment (SORCE). Figure 9 compares the various irradiance data sets acquired from these missions. Offsets among the data sets reflect the different radiometric scales of the individual measurements. Since late 1978 at least two inde-

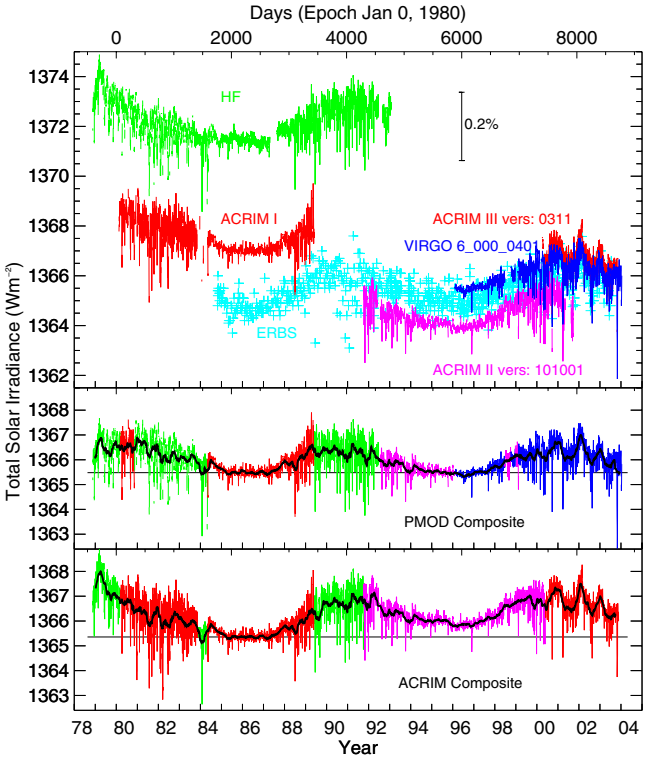

Fig. 9. Compared in the top panel are daily averaged values of the Sun's total irradiance from radiometers on different space platforms since November 1978: HF on Nimbus 7 [57], ACRIM I on SMM [140], ERBE on ERBS [84], ACRIM II on UARS [141], VIRGO on SOHO [43], and ACRIM III on ACRIM-Sat [143]. The data are plotted as published by the corresponding instrument teams. Note that only the results from the three ACRIM and the VIRGO radiometers have inflight corrections for degradation. Shown in the two bottom panels are the PMOD [38, 39, 44] and ACRIM [142,146] composite irradiance time series compiled from the individual data sets together with a 81-day running average. The differences between the two composites are discussed in the text

pendent solar monitors have operated simultaneously in space. Currently operating are radiometers on SOHO, ACRIMSAT and SORCE.

The two composite irradiance records also shown in Fig. 9 are compiled from multiple, cross-calibrated independent measurements [38,39,44,142,146]. Both composite records use Nimbus 7 and ACRIM data prior to 1996 but in one time series (designated as the PMOD composite) the VIRGO data from SOHO are used after 1996 [46], whereas the other time series (designated as the ACRIM composite) relies primarily on ACRIM data [146]. Each TSI composite exhibits a prominent 11-year cycle of peak-to-peak amplitude 0.085 % (difference between September 1986 and November 1989 monthly means). Larger fluctuations are evident, and are associated with the Sun's 27-day rotation on its axis. During epochs of high solar activity these shorter term fluctuations corre-

spond to irradiance decreases of a few tenths of a percent whereas near solar minimum the decreases are much smaller.

According to the PMOD composite irradiance record in Fig. 9b, levels of irradiance during the two minima of 1986 and 1996 are similar. This suggests that TSI does not have a significant long-term trend underlying the 11-year cycle during the last 3 decades. Combining the data sets with different assumptions about their long-term stabilities produces a different composite record in which solar irradiance during 1990 to 1992 increases by 0.04 % as shown in Fig. 9c. Willson [142] and Willson and Mordvinov [146] interpret this change as evidence for secular irradiance changes in addition to the 11-year cycle.

An individual radiometer measures irradiance with a typical uncertainty (accuracy) of order 0.2 %, which is insufficient to determine even the change of ≈ 0.1 % that occurs during an 11-year solar activity cycle. Measurement repeatability (precision) is much higher, and adequate for monitoring short-term changes, but retrieving long-term behaviour is more difficult. Careful tracing of the observational databases to each other is crucial. This requires not only cross-calibration of different absolute radiometric scales but also reliable knowledge of the degradation and operating environment (thermal, pointing, etc.) of each individual radiometer in space.

Only the ACRIM, VIRGO and SORCE instruments have the ability to determine exposure-dependent sensitivity drifts by on-board comparisons with redundant radiometers that receive less solar exposure. Because of this, the PMOD composite relies primarily on the measurements made by ACRIM I on SMM, ACRIM II on UARS and VIRGO on SOHO. The Nimbus 7 Hickey-Frieden (HF) radiometer observations are used to place ACRIM I and ACRIM II data (which do not overlap in time) on a common radiometric scale, which is then adjusted to the Space Absolute Radiometric Reference (SARR) scale [20]. Figure 10 shows the deviations of the original data from the PMOD composite in Fig. 9 and illustrates the most important corrections applied to the original data. Fröhlich and Lean [44,45] and Fröhlich [38,39] provide a detailed description of the corrections, which are summarized in the following.

Significant corrections are applied to the NIMBUS 7 HF measurements to account for sensitivity changes at the beginning of the mission (before 1980 and during the spin-mode period of SMM) and, more importantly, near the end of the mission from 1990 to 1992. This latter period coincides with the gap between the ACRIM I and II data. A variety of independent studies suggest that the HF radiometer experienced notable sensitivity changes. Comparisons with both the ERBE data [85] and models based on ground based observations [17] indicate two discontinuities of -0.31 and $-0.37\,\mathrm{W\,m^{-2}}$ near 1 October, 1989 and 8 May, 1990, respectively. The second jump is difficult to identify and may reflect the continuation of sensitivity drifts identified by comparison with ACRIM I [41,46] earlier in the record. The change in the Nimbus 7 sensitivity during the ACRIM I to ACRIM II gap is determined as -617 ± 50 ppm (≈ 0.06 %).

In the PMOD composite construction, the *corrected* HF data are then used to adjust ACRIM II measurements to the scale of the ACRIM I measurements and the original ACRIM II data are shifted by $+2149 \pm 33$ ppm. The only correction made to ACRIM I data is during 1980 when a time-allocation of the degradation different from that published by Willson and Hudson [145] is applied (as described in [44]). This correction is evident in Fig. 10 as a small linear decrease of ACRIM I data relative to the PMOD composite.

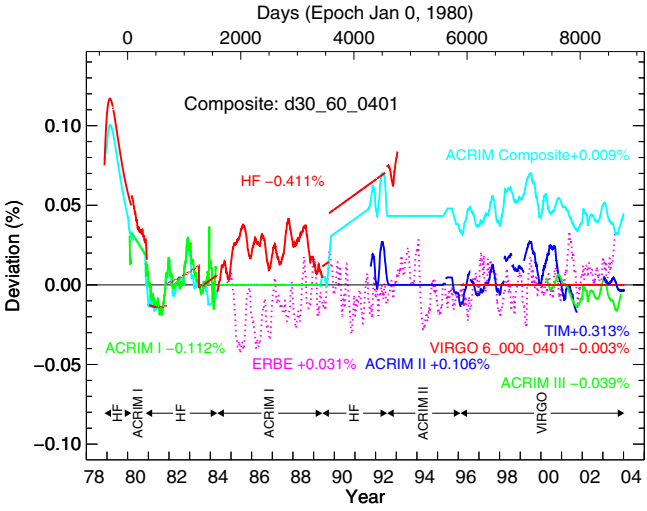

Fig. 10. Shown are differences of the PMOD total solar irradiance composite to the original data sets. Smooth lines indicate that the radiometer is the basis for the composite and if coincident with zero that only an overall scale shift has been applied (ACRIM I after 1984, ACRIM II and VIRGO). The largest corrections are applied to the HF record, as summarized in the text. For the ACRIM I record in 1980 the original correction published by Willson and Hudson [145] was revised slightly, as described in [44]. Also shown are ratios of the ACRIM composite [142,146] to the PMOD composite. It is evident in these ratios that the primary difference between the PMOD and ACRIM composites is due to the omission in the ACRIM composite of the HF correction during the gap between the ACRIM-I and II data sets in the period from 1990–1992

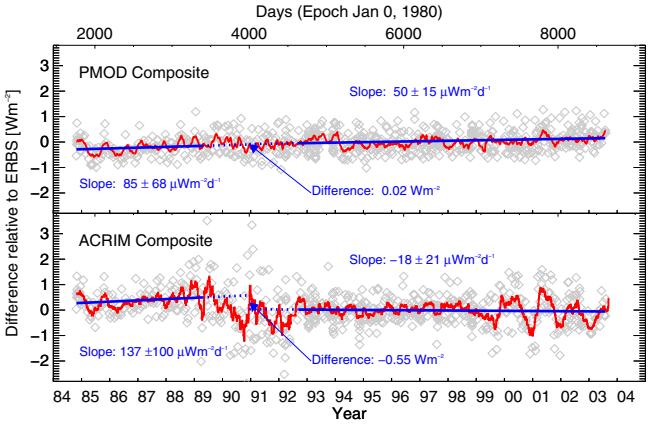

Fig. 11. Shown are the ratios of the PMOD and ACRIM composite TSI records to the independent ERBS observations. The main difference is localized in the gap between the ACRIM I and ACRIM II missions. It is unlikely that ERBE instrumental effects can explain these differences as Willson and Mordvinov [146] suggest, since this would require an episodic sensitivity change confined only to this period

The VIRGO radiometers used in the PMOD composite are also corrected for long-term sensitivity changes, related to their solar exposure (for details see, e.g., [39].

The ACRIM composite[1] shown in Fig. 9c differs from the PMOD composite[2] primarily because in the former the Nimbus 7 HF data are used without any corrections to place ACRIM I and ACRIM II data on a common radiometric scale. This is confirmed in Fig. 11 where comparison of the two different composites with the independent ERBE data reveals distinct differences mainly in the 1990 to 1992 period, i.e., during the gap between the ACRIM I and ACRIM II data sets. Since the ERBE radiometer has had minimal solar exposure (equivalent to about 2 days during its 17 years of operation) its sensitivity drifts are expected to be small. The increase of 18.2 ppm/year seen in Fig. 11 relative to the PMOD composite amounts to a total change over the 17 years of 310 ppm, or an increase of about 150 ppm per exposure day. This increase may be analogous to the sensitivity increase observed in the PMO6V radiometers early in the mission, which are about 70 ppm per exposure day. Neither the PMOD composite nor the ERBE data supports the claim of Willson and Mordvinov [146] that the ERBE radiometer has degraded primarily during 1990 – 1992 (a speculated consequence of high solar activity levels), nor that solar irradiance has undergone significant secular changes in recent decades. The slope of the ratio to the PMOD and ERBE TSI time series suggests that the uncertainty of the long-term behaviour of the composite TSI is about ± 60 ppm per decade. Alternatively, the uncertainty is estimated as ± 92 ppm by adding the uncertainties related to the tracing of ACRIM II to I together with the HF corrections. Thus, any change of TSI between the two recent solar minima can be regarded as zero with a high level of confidence.

3.2. Characterization of TSI variability in the frequency domain

Fourier-transforming the TSI time series produces the power spectrum shown in Fig. 12, which characterizes total solar irradiance variance in the frequency domain. The power spectrum of the daily values (using the PMOD composite), shown as the red line in Fig. 12, extends to 5.8 μHz, the Nyquist frequency for 1-day sampling, and has an inherent frequency resolution of 1.3 nHz, afforded by the length of the time series of nearly 24 years (more than 8700 days). To better characterize the solar cycle peak, the plotted spectrum is 3 times over-sampled and yields a peak-to-peak amplitude of 670 ppm at 9.89 years for solar cycles 21–23. The two peaks in the power spectrum near a 1-year period (peak-to-peak amplitude of 126 ppm at 1.09 year and 81 ppm at 0.96 year) are only marginally significant.

VIRGO data with 1-minute sampling allow an extension of the TSI power spectrum to higher frequencies, where significant power is evident near 5 minutes. Since VIRGO

[1] The ACRIM composite and the ACRIM I, II and III data sets are available from http://www.acrim.com/Data%20Products.htm.

[2] The PMOD composite and VIRGO TSI are available from http://www.pmodwrc.ch/pmod.php?topic=tsi/composite/SolarConstant and http://www.pmodwrc.ch/pmod.php?topic=tsi/virgo/proj_space_virgo as daily values and in the case of VIRGO also as hourly values. VIRGO version 6_000_0401 is used for the PMOD composite in Fig. 9b.

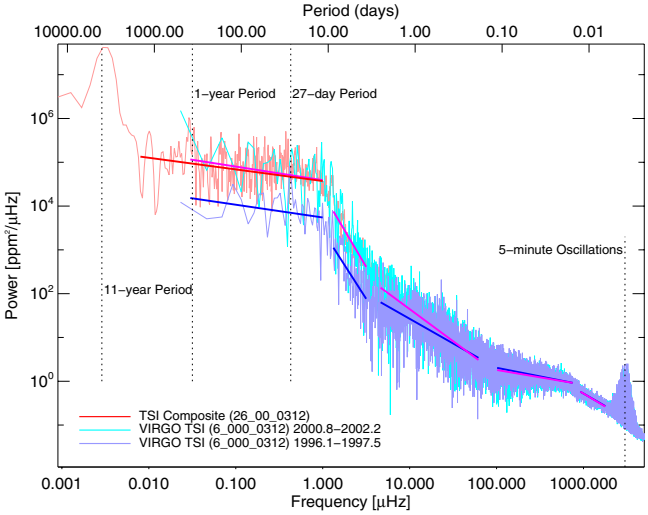

Fig. 12. Shown is the power spectrum of the composite record of daily total solar irradiance for the period from 1978 until 2002 (red). To illustrate the solar cycle variability in the frequency domain, the power spectra of data from VIRGO during solar minimum (Feb. 1996–Aug. 1997) are compared to that of solar maximum (Oct. 2000–Feb. 2002). The solar cycle influence is evident in the differences in power at low frequencies

data now cover more than half a solar cycle, they allow quantification of activity related irradiance changes in the frequency domain from the 5-minute oscillations to periods up to 1000 days. In Fig. 12 the power spectrum for the period 2000.8 – 2002.2 corresponds to high solar activity while that for 1996.1–1997.5 to solar activity minimum. The two power spectra overlap at the highest frequencies but begin to deviate in the region of supergranulation; the difference gradually increases towards lower frequencies reaching more than an order of magnitude in the vicinity of the nominal 27-day rotational period (see also Fig. 17).

In addition to the two distinct peaks at 11 and 1 year, and the peaks of the solar oscillations in the 5-minute range, the power spectrum in Fig. 12 displays turning edges due to characteristic time scales or frequencies where the constant power at low frequency starts to decrease (often termed as 3-db points). The following characteristic time scales are identified with their approximate turning points and average (for minimum and maximum activity) exponent of slopes (slope in double logarithmic scale): 27-day rotational period ($\approx$ 0.68 μHz): -3.3, supergranulation ($\approx$ 6.2 μHz): -1.3, mesogranulation ($\approx$ 56 μHz): -0.4, and granulation ($\approx$ 825 μHz): -1.2.

3.3. Spectroradiometry from space

Space-based observations of solar spectral irradiance have concentrated primarily on measurements at UV wavelengths. The terrestrial atmosphere absorbs solar radiation at these wavelengths (see Fig. 3), and knowledge of its variability is sought to understand stratospheric and ozone fluctuations. Heath and Thekaekara [55] summarize the database

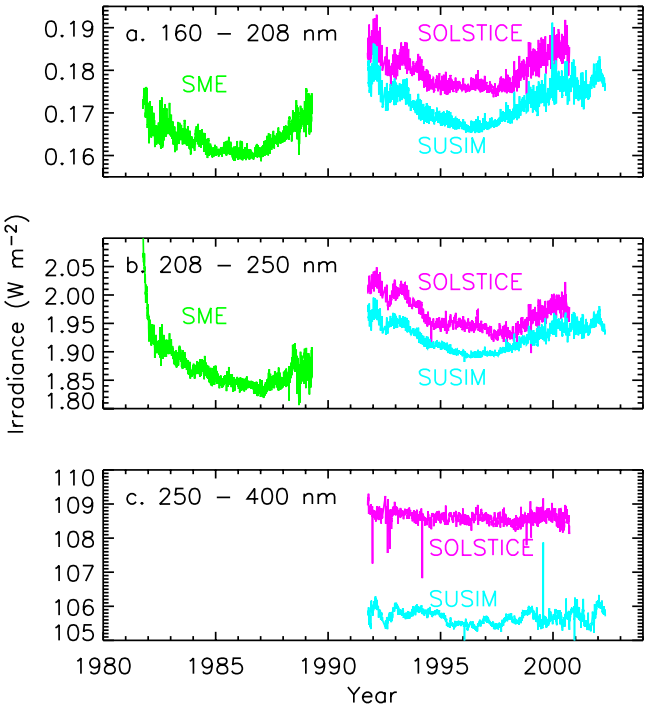

Fig. 13. Shown are space-based observations of solar UV spectral irradiance in selected broad bands at **(a)** 160 to 208 nm, **(b)** 208 to 220 nm, and **(c)** 250 to 400 nm, indicating UV irradiance increases in phase with the solar activity cycle (see also Fig. 2 which includes also a plot of the UV irradiance in the range 160 to 208 nm)

of the early measurements from space, in which instrumental effects obscured true variability. Currently the longest and most reliable data are the measurements made by the Solar Stellar Irradiance Comparison Experiment (SOLSTICE) and the Solar Ultraviolet Spectral Irradiance Monitor (SUSIM) on UARS, since October 1991 [24]. Prior to UARS, the Solar Mesosphere Explorer (SME) monitored the UV irradiance with lesser accuracy and precision. The UARS and SME data, examples of which are shown in Fig. 13, suggest solar cycle irradiance changes of 20 %, 8 % and 3 % near 140, 200 and 250 nm, respectively [81, 113, 115].

Figure 14 shows current understanding of solar spectral irradiance variability during the 11-year solar cycle in terms of percentage changes relative to the irradiance, and also as energy changes. Rotational modulation of spectral irradiance is superimposed on the solar cycle variations at all wavelengths, in phase with solar activity in the UV spectrum, transitioning at wavelengths from 300 to 400 nm to TSI-type anti-phase fluctuations at visible and infrared wavelengths. Although the spectral irradiance energy changes sum to produce the TSI changes in Fig. 2, the actual energy changes in the spectrum are not well constrained. The variability amplitudes in the UV spectrum shown in Fig. 14 are derived from UARS observations [81] but the spectrum changes shown at wavelengths longward of 400 nm are theoretical estimates [124, 132].

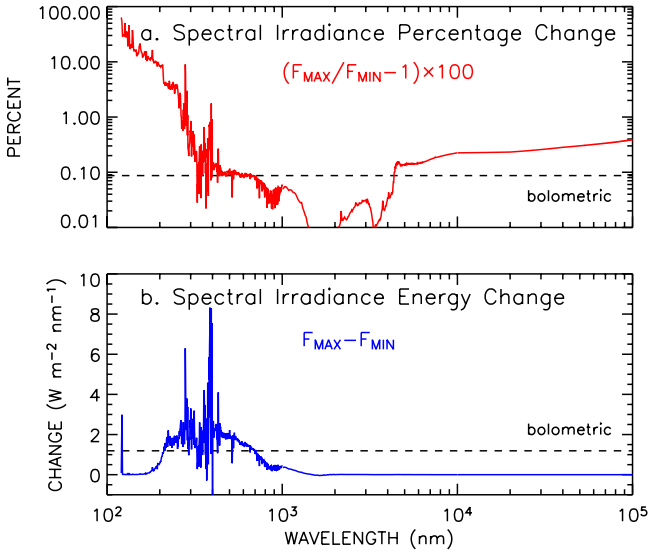

Fig. 14. The spectrum variations that cause the changes in total solar irradiance are shown in **(a)** as ratios of spectra at high and low solar activity, respectively (F_{MAX}) and (F_{MIN}), and in **(b)** as their difference in energy units. The variability amplitudes in the UV spectrum are derived from UARS observations [81] and the changes for wavelengths longward of 400 nm are theoretical estimates [124, 132]

Solar UV spectral irradiance monitors, such as those flown on UARS and SME, utilize various combinations of filters, gratings and mirrors to select, disperse and focus the solar spectrum into sub-nanometer resolution. Photomultipliers or photodiode detectors record the dispersed spectrum. Both SOLSTICE and SUSIM on UARS (and also SOLSTICE on SORCE) have absolute uncertainties approaching ±6 %, depending on wavelength. Differences between the SOLSTICE and SUSIM spectral irradiances, such as in Fig. 13, are within these uncertainties for 5 nm bands. SME irradiances have larger uncertainties, of order ±15 %, and are shown in Fig. 2 scaled to match the UARS irradiance scale.

As with total irradiance radiometers, exposure to solar radiation can alter the overall sensitivity of UV spectroradiometers by changing the transmittance and reflectance of optical surfaces. SOLSTICE and SUSIM on the UARS aim to achieve long-term repeatability of a few percent by incorporating in-flight sensitivity tracking to correct their signals for instrumental drifts. SOLSTICE accomplishes these corrections by regular comparisons with signals from a collection of bright blue stars. SUSIM uses deuterium lamps and redundant optical elements to quantitatively estimate the impact of exposure-related degradation on its multiple optical surfaces. [148] describe validations and comparisons of SOLSTICE and SUSIM observations.

Observations of solar cycle spectral irradiance variability at visible and infrared wavelengths are lacking because, until the launch of the SORCE mission in 2003, space-based spectroradiometers had neither the sensitivity nor long-term stability necessary for the detection of variations on time-scale of the solar cycle or longer. Real variability

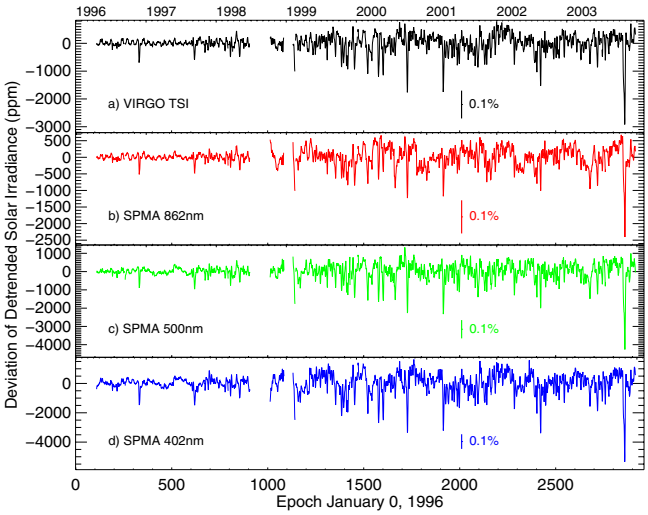

Fig. 15. Time series from SOHO/VIRGO of detrended TSI (**a**) and the three channels of filter-radiometers (**b–d**) show coherent modulation with increasing amplitude during epochs of higher solar activity

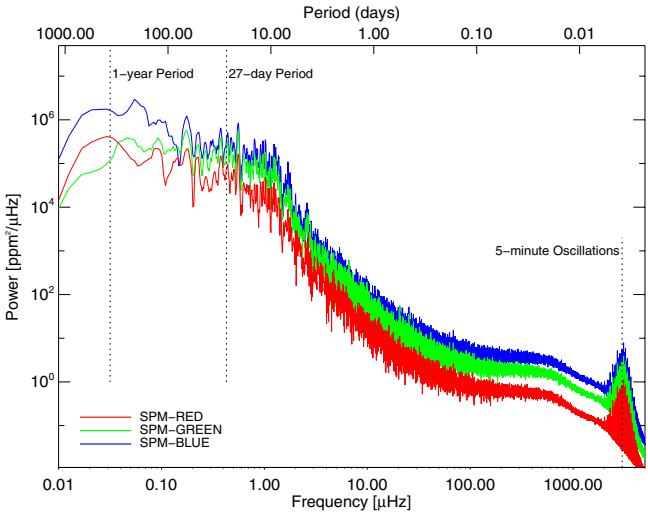

Fig. 16. Shown are power spectra of the detrended spectral irradiance data measured by the SOHO/VIRGO filterradiometer channels from 1996 until December 2003

in the solar visible and infrared spectrum has nevertheless been detected on shorter time scales from observations by filter radiometers on Nimbus 7 [81], on EURECA by the SOVA2 SPM [19] and on SOHO by the VIRGO SPM channels in three 5-nm bands, centered at 402 nm, 500 nm and 862 nm [42]. The latter data show modulation up to periods of about one year in detrended solar irradiances [40]. The variations are compared in Fig. 15 with TSI variations, with all data sets detrended by subtracting

polynomials of the same degree. Variability, which can be reliably assessed at periods $\lesssim$1 year, decreases in the visible spectrum with increasing wavelength, from 465 ppm near 400 nm to 170 ppm near 800 nm. This may be compared with the TSI variance of 185 ppm for the same period of time. This decrease is qualitatively consistent with the theoretical estimates from [124, 132] (Fig. 14) which show that solar cycle variability amplitudes in the visible part of the spectrum also decrease with increasing wavelength.

The power spectra of the three VIRGO channels shown in Fig. 16 are qualitatively similar to that of TSI in Fig. 12. Spectra for active and quiet Sun are compared in Fig. 17 together with the corresponding ratio for TSI. The most interesting feature in Fig. 17 is the dip at the 27-day period which indicates that the rotational modulation is only weekly dependent on the level of solar activity. Towards higher frequencies the ratio first increases until a maximum at about 10 days, then decreases to a constant value slightly above one for periods shorter than a few hours. The different behaviour of the visible (green) and near UV (blue) channels at periods longer than the rotational period probably reflects the detrending method, and may not be of solar origin. Note that the ratios at frequencies above 200 μHz, in the region of the granulation and mesogranulation, are unexpectedly different from unity, with values of 1.15, 1.19, 1.18 for the red, green and blue channels and 1.21 for TSI, respectively.

Figure 18 shows the relative contributions to TSI variability of spectral irradiance in the three different VIRGO wavelength bands, as determined from multivariate frequency analysis (see, e.g., [64, Chapters 5.6f, 8.4f]). In the frequency range from 0.29 to 1.65 μHz (periods of 7 to 40 days) the explained variance reaches 97 % with a share between the colours of 12, 25 and 60 % for the infrared (red), visible (green) and near UV (blue) channels, respectively. It is interesting to note that for the same range the red and blue channel are more or less in phase with TSI whereas the green channel lags by about 30 degrees [40].

3.4. Limitations of present solar monitoring capability

The cluster of recently-measured total solar irradiance values near 1365.5 W m^2, evident in Fig. 9 by the lower spread in the absolute scale of observations since about 1990, suggests that the accuracy of TSI measurements has improved significantly relative to the measurements made 20 years earlier. In spite of this apparent improvement, the problem of absolute accuracy remains an important issue, as does the determination of the long-term measurement stability (see, e.g., [106]). In particular, preliminary SORCE TSI measurements [71] are about 4 W m^{-2} lower [65] than the values of the PMOD composite which is referred to SARR [20]. This difference exceeds the combined stated uncertainties, for reasons unresolved as yet.

A demonstrated capability for radiometric accuracies at least a factor of 10 better than currently possible is urgently needed to establish a benchmark for future solar irradiance monitoring. In lieu of this, overlap by successive radiometers remains essential for cross tracking of radiometer calibrations to achieve the needed long-term precision. For this reason, producing a reliable long-term composite record requires at least two independent experiments simultaneously in space. Although more than one space-based TSI instrument is planned during the next few years, this may not be the case in the extended future. For the spectral irradiance at near UV, visible and near IR wavelengths,

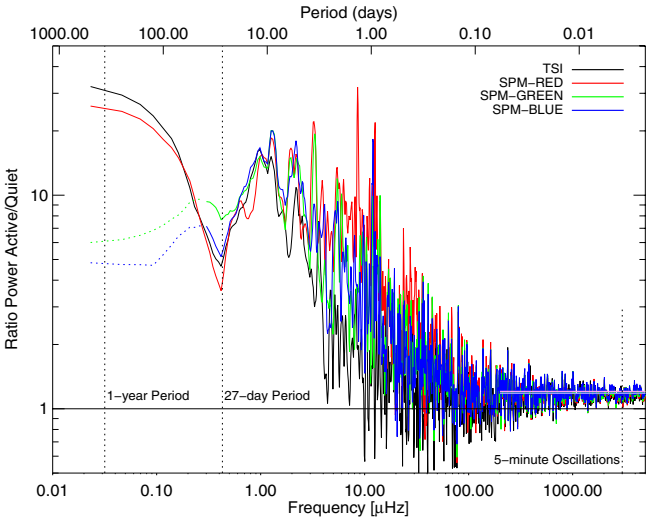

Fig. 17. Ratio of the active (2000.8–2002.2) to quite (1996.1–1997.5) power spectra of TSI and the detrended channels of filterradiometers (data sets from SOHO/VIRGO). The reason for the different behaviour of the green and blue channel from that of TSI and the red channel is probably due to instrumental effects not removed during the period of solar minimum. The ratio at high frequencies ($> 200\,\mu$Hz, as indicated by the horizontal lines) amounts to 1.15, 1.19, 1.18 and 1.21 for TSI, the red, green and blue channels, respectively

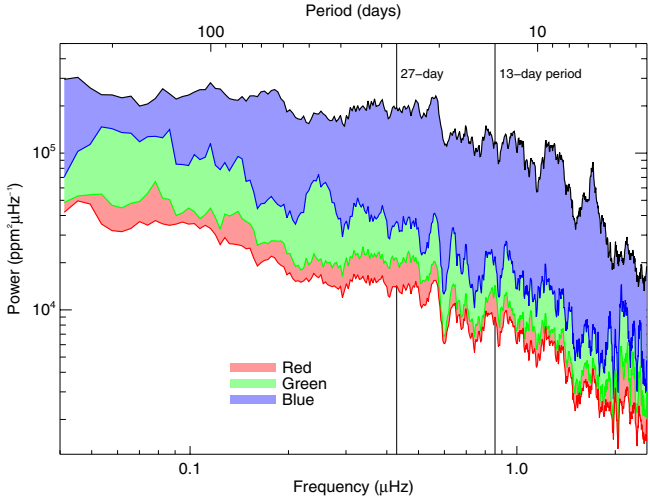

Fig. 18. Shown are results from a multi-variate frequency analysis of VIRGO's three spectral irradiance (SPM) channels relative to total solar irradiance (TSI). The top curve is the power of TSI and the shaded areas indicate that part explained by the spectral irradiance in each of the three different spectral bands

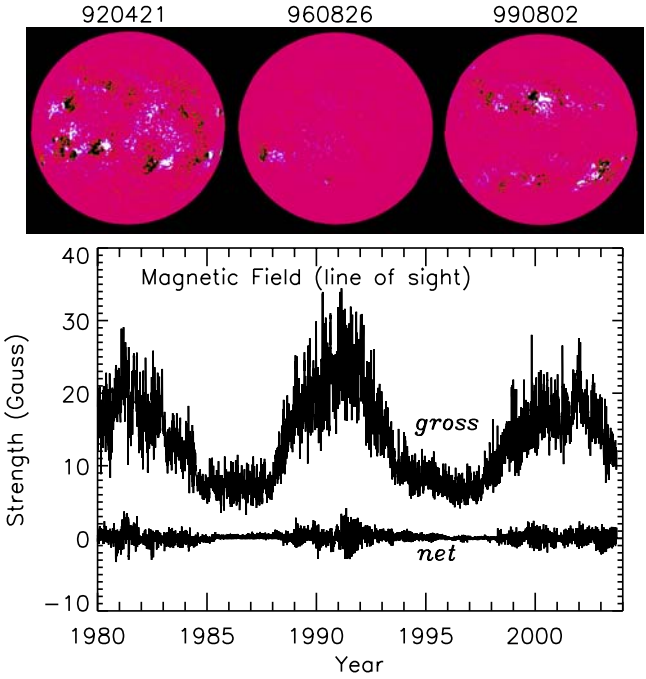

Fig. 19. Variations in the Sun's gross and net magnetic flux are shown during the epoch of space-based irradiance measurements in the lower diagram. The time series are obtained from the unsigned sum and signed sum, respectively, of magnetic flux in images made by the National Solar Observatory, such as those shown for three different periods in the upper panel. In these magnetograms, light and dark areas signify regions of opposite polarity

the situation in terms of long-term stability is even less satisfactory. New, accurate in-flight techniques for assessing the long-term instrumental changes are needed. Hopefully, the novel approaches now being utilized by instruments on the SORCE mission [52,71, 114,147] will produce spectral irradiance time series with significantly higher long-term repeatability than has been achieved thus far.

4. Sources of irradiance variability

Solar radiative output undergoes distinct, wavelength-dependent variability with amplitudes and time scales that relate closely to the level of the Sun's activity. Solar activity, initially detected in sunspot observations in the mid nineteenth century (Fig. 1), is now known to originate in a cycle of magnetic flux driven by a dynamo seated near the bottom of the convection zone, at $\approx 0.7 R_{\odot}$ (e.g., [25]). This flux produces a variety of features, such as sunspots, faculae and plages (Fig. 7), and coronal holes, and instigates numerous solar phenomena, including irradiance and solar wind fluctuations, flares and coronal mass ejections.

During times of high solar activity substantially more magnetic flux pervades the solar atmosphere than during quiet conditions at solar minima. Figure 19 shows the

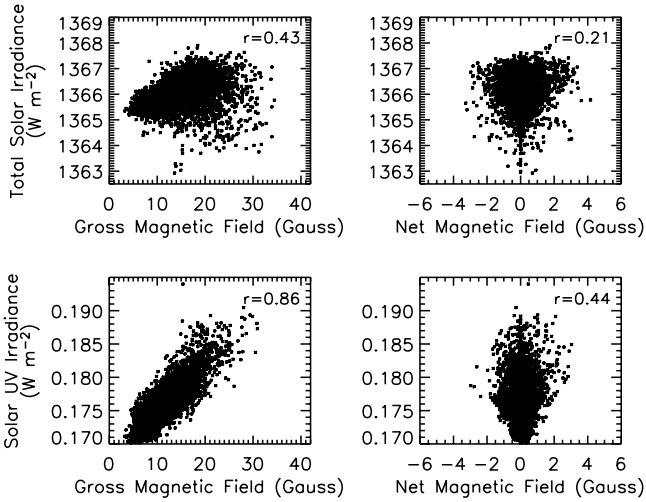

Fig. 20. Shown are scatter plots of daily mean solar irradiance, from Fig. 2, with total (net and absolute) magnetic flux, from Fig. 19. In the upper panel, the scatter plots of total irradiance and magnetic flux illustrate a distinctly non-linear relationship. UV irradiances (160–208 nm) have a more linear relationship with magnetic flux, as the scatter plot in the lower panel demonstrates

variations in magnetic flux during recent 11-year cycles, as disk-averages of both the absolute and signed quantities. But although the solar magnetic cycle is the ultimate driver of irradiance variations, the scatter plots in Fig. 20 show that solar irradiance correlates poorly with the net and disk-averaged magnetic flux; with a correlation coefficient of 0.43 for unsigned flux and 0.21 for signed flux versus TSI, only 18 and 4 % of the variance is explained. Changes in specific magnetic features, rather than in the net- or disk-averaged magnetic flux, relate better to irradiance variability.

Magnetic fields in the solar atmosphere produce at least two types of features that cause significant variations in solar irradiance. These features are evident in the solar images in Fig. 7. Sunspots, which are cooler (see Fig. 4) and darker than the surrounding solar atmosphere, are evident in the red continuum images. Faculae, which are hotter (see Fig. 4) and brighter, are seen primarily on the limb of visible-light images; the Ca K images reveal their overlying chromospheric counterparts, the plages. Sunspots and faculae, respectively, deplete and enhance local solar radiance, thereby altering the net radiation projected in the direction of the Earth, i.e., the irradiance. Since sunspots and faculae typically occur on the Sun together, a competition of their relative strengths, which are strongly wavelength-dependent, determines solar irradiance variability. For example, while sunspots produce significant depletions in the visible and infrared spectrum, evident by the reduced total solar irradiance near 1999.6 in the time series in Fig. 7a, they have minimal effect in the UV spectrum, where no depletion of UV irradiance in Fig. 7b occurs at that time.

Modulation by sunspot darkening causes prominent reductions in total solar irradiance on time scales of solar rotation. TSI brightening associated with the largest, contiguous facular regions (those associated with chromospheric plages) also occurs, but with notably smaller amplitudes than the sunspot-related reductions. The net effect

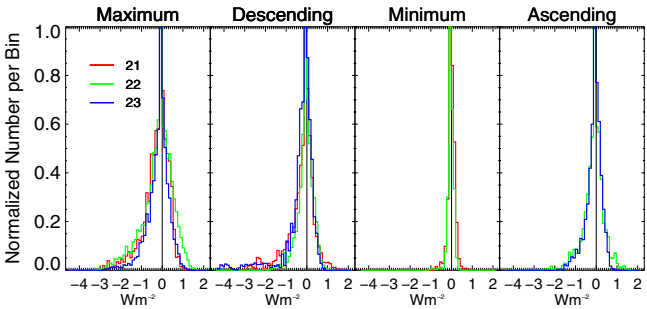

Fig. 21. Histograms of TSI values are shown for different phases of solar cycles 21–23. The histograms are averaged over the following periods: maxima of cycle 21: 1979.2 . . . 1982.0, cycle 22: 1989.3 . . . 1992.1, and cycle 23: 2000.0 . . . 2003.1; descending part of cycle 21: 1982.0 . . . 1985.3, cycle 22: 1992.1 . . . 1995.3, and cycle 23: 2003.1 . . . 2003.9; minima of cycle 21/22: 1985.3 . . . 1987.4, and cycle 22/23: 1995.3 . . . 1997.6; ascending part of cycle 22: 1987.4 . . . 1989.3, and cycle 23: 1997.6 . . . 2000.0.

of these two competing variability sources explains why, on average, periodograms of TSI lack significant power near the rotational modulation period [34] and suggest a reason why rotational modulation is not strongly dependent on solar activity (Fig. 17). In the UV spectrum (below 300 nm), however, rotational modulation arises primarily from the influence of facular features which are comparatively much brighter than sunspots are dark at UV wavelengths: UV irradiance time series have significant power near the rotational modulation period [80].

Enhanced emission from bright magnetic features that have smaller spatial scales than the largest contiguous faculae and are more dispersed on the solar disk (typically tracing the boarders of the chromospheric network) contribute additional variability to both total and UV irradiance during the solar cycle [29, 35, 79]. Other sources of solar cycle irradiance variability are also postulated, such as a change in photospheric temperature [49, 67]. Whether 'non-facular' variations result from, or are independent of, solar magnetic features (e.g., thermal shadows, active network) is not yet clarified.

Distributions of daily TSI values, such as those shown in Fig. 21, help quantify the relative influences of magnetic features. As sunspots and faculae, respectively, decrease and increase the irradiance, each influences the distribution on opposites sides of its maximum, called the mode, in a distinct way. Figure 21 shows the mean distributions for maximum, decreasing, minimum and ascending phases of the solar cycle. As expected, except during solar minimum the distributions are asymmetric, with an extended tail of lower values, especially during times of higher activity, associated with sunspots.

The distributions in Fig. 21 can help characterize the mean influence of sunspots and faculae at different solar cycle phases. They show, for example, that the ratio of the sunspot and facular effects changes during the solar cycle. The average ratio is 1.77 ± 0.58 according to the mean of the negative and positive differences to the mode. The standard deviation of the ratio is mainly determined by changes over the solar cycle with a maximum ratio of 2.24 during the descending part and a minimum of 1.18 during solar minima.

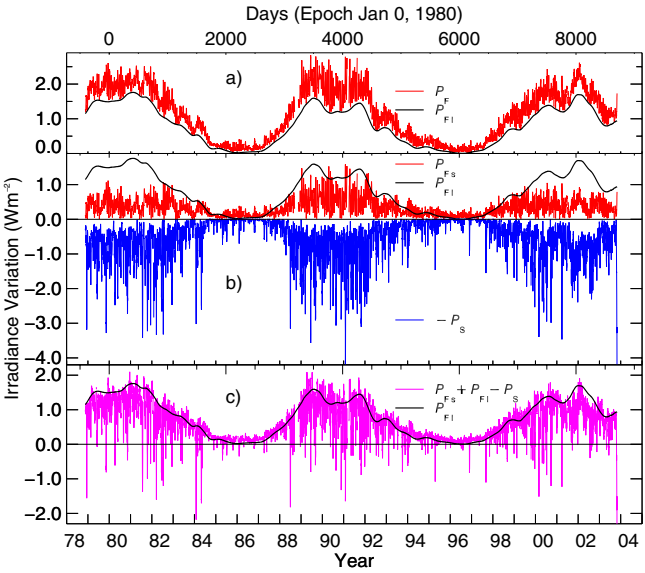

Fig. 22. Models of total solar irradiance variability that combine the influences of sunspot darkening and facular brightening can account for a significant fraction of the observed variance in the total solar irradiance composite record. Shown in **(a)** is the facular influence P_F together with P_{Fl} determined as the lower envelope of P_F. Shown in **(b)** is P_{Fs}, P_{Fl} and $-P_S$, and in **(c)** the net effect on total solar irradiance of the combined sunspot and facular changes (all calibrated by linear regression against the PMOD composite)

5. Empirical models of magnetic sources of irradiance variability

Information about the two primary sources of irradiance variability, sunspots and faculae (associated with both plages and active network), is available from a variety of solar observations which enable the quantitative modelling of irradiance variability independently of direct measurements. The daily facular brightening, P_F, and sunspot darkening, P_S, time series shown in the upper panel of Fig. 22 since 1976 are two indices that are used widely for this purpose. The facular brightening index is a composite of directly measured flux ratios of emission from the center of Fraunhofer features, primarily the MgII h & k index, (e.g., Figs. 5 and 8) relative to emission in the line wings [23,83,138]. White light solar images that record the locations and areas of sunspots, such as in Fig. 7, provide the primary inputs for the sunspot darkening index.

5.1. Sunspots

Sunspot darkening, the fractional change in irradiance caused by sunspots, is calculated explicitly (in this case for total irradiance) as

$$P_S = \sum \Delta S/S_Q = \sum \mu A_{WDC}(C_S - 1)\frac{R(\mu)}{\int_0^1 R(\mu)\mu d\mu} \tag{3}$$

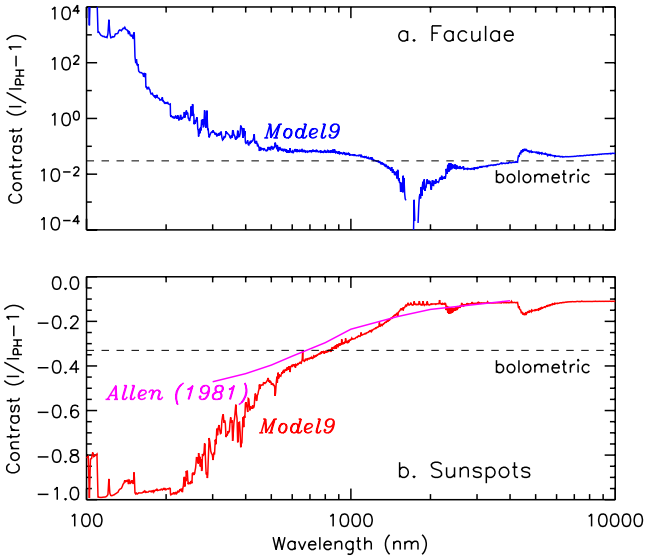

Fig. 23. The contrasts of **(a)** bright faculae and **(b)** dark sunspots are shown as functions of wavelength from the UV to the IR spectral regions. The contrasts are ratios of the radiance of these features to that of the background photosphere, determined from theoretical calculations with the radiative transfer code ATLAS9 from [68] by [131] and limited observations [4]

where ΔS is the reduction in irradiance relative to the quiet Sun, S_Q, for a sunspot of area A_{WDC} (in fractions of the solar hemisphere) at location μ in heliocentric coordinates. C_S is the sunspot's contrast (ratio of spot emission to the background quiet photosphere) and $R(\mu)$ is the center-to-limb variation function which is assumed to be the same for the quiet photosphere and the spot. The summation is over all spots on the solar disk at a specific time, and utilizes bolometric contrast and center-to-limb functions (Eddington limb darkening $R(\mu) = (3\mu + 2)/5$) appropriate for modelling total solar irradiance variations. Ground-based white light images made from 1882 to 1976 by the Greenwich Observatory, and most recently by the U.S. Air Force operational Solar Observation Optical Network (SOON) sites [3] supply the basic time-dependent information about sunspot areas and locations. Greenwich sunspot areas are reported to be 20 % larger than SOON sunspot areas [27]. The time series shown in Fig. 22b, is the energy reduction in total radiative output caused by sunspot darkening, P_S, calculated from SOON sunspot data and calibrated by linear regression against the PMOD composite.

Sunspots in reality comprise a very dark central umbra and a less dark surrounding penumbra but present versions of P_S do not include this distinction because the SOON data lack sufficient information about these specific sunspot features. Sunspots also have wavelength-dependent contrasts. As Fig. 23 shows, they are factors of 3 to 5 darker in the UV spectrum than in the IR spectrum. The bolometric sunspot contrast takes this into account by weighting the contrast spectrum (e.g., Fig. 23) with the solar spectrum

[3] The observations of the sunspot regions are available from the National Geophysical Data Center (NGDC) operated by the National Oceanographic and Atmospheric Administration (NOAA) at Boulder, Colorado, http://www.ngdc.noaa.gov/stp/SOLAR/ftpsunspotregions.html.

(e.g., Fig. 3). However, the spectral dependence of sunspot contrast has not been well determined, as indicated by the differences between the observational and theoretical estimates in Fig. 23.

5.2. Faculae

The explicit calculation of a facular index, P_F, analogous to P_S is also possible [79] but more difficult because faculae have lower contrasts in the visible spectrum and more fragmented areas than sunspots. In solar images made in the core of Ca and other Fraunhofer lines (e.g., Fig. 7) the emission is preferentially enhanced in chromospheric plage and bright network that overlie photospheric faculae. Ca images therefore provide information about facular areas and locations from which to construct facular brightening indices [53,79]. Faculae can also be identified in magnetograms (e.g., [66]).

Facular indices derived from feature quantification in solar images are difficult to produce over extended periods of time because of the lack of a long-term database of appropriately calibrated images. Furthermore, physical characteristics of faculae and plages such as their center-to-limb variations and contrasts are less well known than for sunspots. This motivates the use of alternative facular indices such as the Mg-II index, which consists of the ratio of the core and wing fluxes and minimizes the influence of instrumental drifts. The line cores originate in the chromosphere where bright features have greater contrast than their photospheric counterparts (a factor of 2 versus a few percent for an active region), and the flux measurements automatically integrate emission over the full disk. One disadvantage is that chromospheric and photospheric radiances can have different center-to-limb dependence of emission and contrast.

5.3. Models of contemporary irradiance variability

Empirical models of solar irradiance variability over multiple time scales utilize as inputs the sunspot darkening and facular brightening indices, P_S and P_F, combined in different proportions for total versus spectral irradiance at different wavelengths. Historical reconstructions may utilize an additional third index of postulated long-term variability. The models are constructed differently depending on whether or not direct irradiance observations are available to establish the relative contributions of sunspots and faculae at the wavelengths of interest, over the time scales of interest.

Models of contemporary total and UV spectral irradiance variability, for which adequate observational databases exist, are developed in one of two ways. Either the P_F and P_S time series are regressed together against the observed irradiance, S or $F(\lambda)$, or the observations are first corrected for sunspot effects then the residual time series, $S - P_S$ or $F(\lambda) - P_S(\lambda)$, is linearly regressed against P_F [44,74,81]. Both approaches yield an expression of the form $S(t) \propto a_{tot} P_S(t) + b_{tot} P_F(t)$ for total solar irradiance or $F(\lambda, t) \propto a_\lambda P_S(t) + b_\lambda P_F(t)$ for spectral irradiance at time t and wavelength λ. Thus, in empirical irradiance variability models the indices $P_S(t)$ and $P_F(t)$ contain time dependent information about the sources of the irradiance variability and the (time-independent) coefficients $a_{\lambda,tot}$ and $b_{\lambda,tot}$ adjust the relative contributions of these sources for radiation at different wavelengths, or for total irradiance. In practice, the

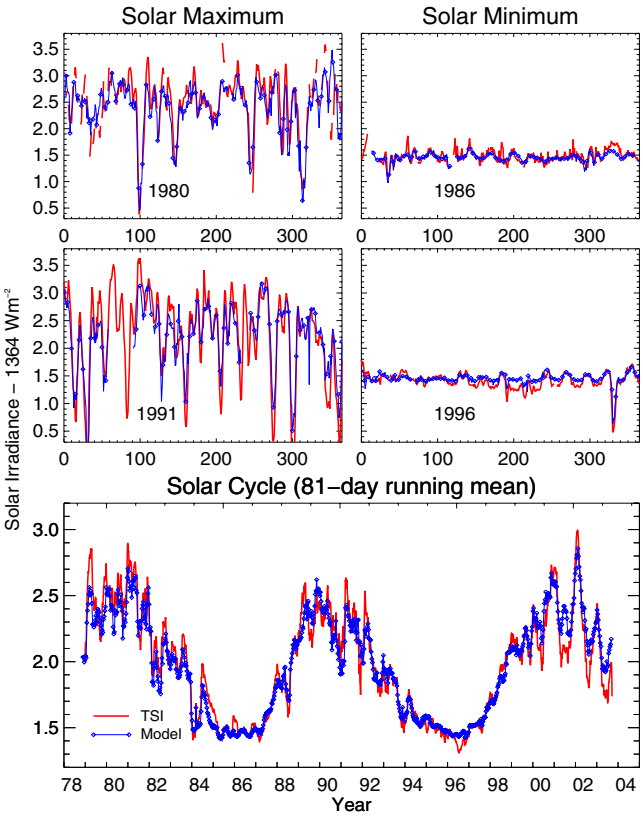

Fig. 24. An empirical model of total solar irradiance variability based on two short-term indices, sunspot darkening and facular brightening, and a long-term index for the solar cycle variations from Fig. 22 is compared with the composite observational irradiance record during solar rotation during high solar activity (upper left panels) and low solar activity (upper right panels). Compared in the bottom panel are the smoothed model and measurements during two solar cycles

observations may or may not be detrended prior to the regression, depending on the confidence (or lack of) in their long-term stability (e.g., [81]).

A model that has two components – sunspot darkening, P_S, and facular brightening, P_F (Fig. 22) – explains 77.2 % of the variance of the total solar irradiance composite record. A further refinement consists of separating the facular component into shorter- and longer-term parts, P_{Fs} and P_{Fl}. The component P_{Fl} is determined as a smoothed lower envelope of P_F, as shown in Fig. 22a, and $P_{Fs} = P_F - P_{Fl}$. Multiple regression against the three indices yields some improvement in the model's reproduction of short-term total irradiance variations, and explains 78.6 % of the variance. This approach better accommodates possible differences in the short and long-term sources of irradiance variability. The fact that the coefficients determined with the three-component model are notably different for the short and long-term facular proxy may indicate differences in the physical sources that produce the longer-term irradiance variations, presumably associated with bright network inside and outside the active regions. Direct observations

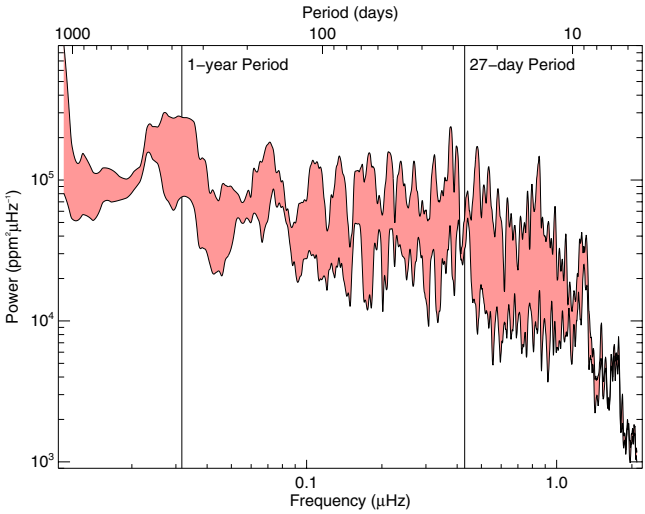

Fig. 25. Results are shown from the bi-variate analysis of observed TSI and the empirical model based on sunspot and facular indices. The top curve shows the power spectrum of TSI and the shaded area shows the part of observed TSI variance that the model explains. Note the lack of correlation at the 27-day rotational period and around 575, 206 and 141 days

from MDI/SOHO of the fractional disk areas of bright features and their contrast as a function of the magnetic field [98,99] indicate that this difference may just be due to the fact that the translation from MgII index to TSI depends on the specific contrast, C/B, of the network and faculae and not on C.

The comparison in Fig. 24 with the PMOD composite TSI record of the three-component model (calibrated over the full period from 1978 to 2003) shows that the model reproduces the observed gross temporal features [40]. However, during activity maxima the modelled sunspot and facular signals show about 25 % higher amplitudes than the deviations from the mode (Fig. 21) recognizes. A more detailed analysis shows that during the descending phases and minima of the activity cycle only the sunspots determined from the model differ, whereas during the ascending parts both methods give similar results. These differences can be explained partly by some direct compensation of darkening by spots and simultaneous brightening by faculae, but may also arise from changes of the spot contrast during the cycle as observed by [90] which the model does not include.

Bi-variate spectral analysis clarifies the frequency dependence of the variance in the observed total irradiance explained by the three-component model. Figure 25 shows that for periods from 13 to 1200 days the mean coherence squared is 0.73 which means that the model explains 73 % of the variance. At some periods the coherence is very low, most prominently near the 27-day rotational period, but also near 575, 206 and 141 days. The comparison in Figure 25 illustrates that the model based on daily sunspots and facular indices can only explain the main features of the actual irradiance variations, but not all details of the variability.

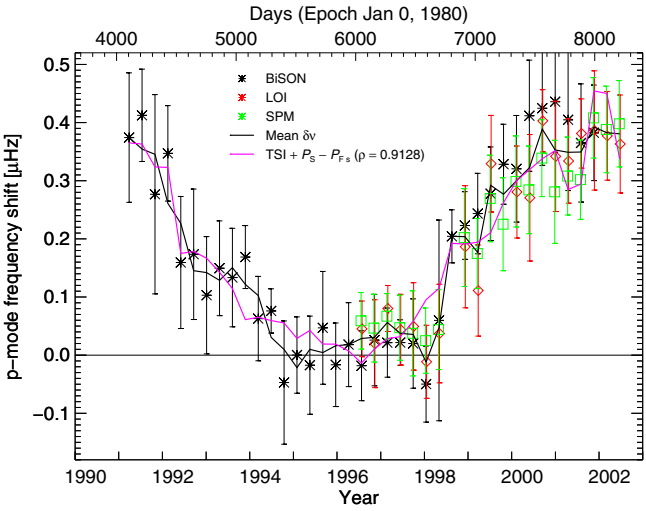

Fig. 26. The correspondence of TSI corrected for the short-term variability with p-mode frequency shifts is shown over a solar cycle. The correlation between the mean of the different observations of the p-mode frequency changes and the corrected TSI amounts to 0.913 with a slope of 0.28 ± 0.015 μHz/W m^{-2}. The data are from the Birmingham Solar Oscillation Network (BISON [16]) and VIRGO/SOHO (e.g., [42])

During the solar cycle, there is a close correlation of the irradiance brightness source with p-mode oscillation modes in the Sun. Figure 26 shows that the solar cycle changes in p-mode frequencies clearly track the residual time series of total solar irradiance corrected for sunspot influences, i.e., the long-term brightening component of irradiance variability. This empirical association may afford a more physical approach for interpreting TSI variability, since these low-degree p-mode oscillations are global in nature and reflect sub-surface processes. However, the mechanisms responsible for this high correlation between the low-degree p-mode frequencies and the facular irradiance signal are not yet understood theoretically, other than by stating that both are related to magnetic field changes. A theoretical explanation for the frequency changes suggests, however, a correlation with opposite sign to that which is observed (e.g., [9]).

At UV wavelengths, empirical models have been developed in a similar way by regression of the sunspot and facular indices against observations [81] and from facular indices determined directly from Ca-K images [79,149]. Figure 27 compares models and observations in three UV bands. The models generally reproduce observed variability better at shorter wavelengths where the changes are larger and less affected by instrument long-term instabilities. For example, a model developed from regression of the P_S and $P_{Fs} + P_{Fl}$ indices in Fig. 22 with detrended SOLSTICE data correlates better with the data at 200 nm (0.88) than at 250 nm (0.7). As Fig. 27 illustrates, there is overall agreement between the model and observations, especially for shorter UV wavelengths on rotational modulation time scales, although less variance is explained than for total irradiance. Wavelength-dependent instrumental drifts may remain in the observations, whose long-term stabilities are still being revised. As well, in the spectral region 250 to 400 nm the precision and stability of the UARS instruments (a few percent) likely exceeds the true

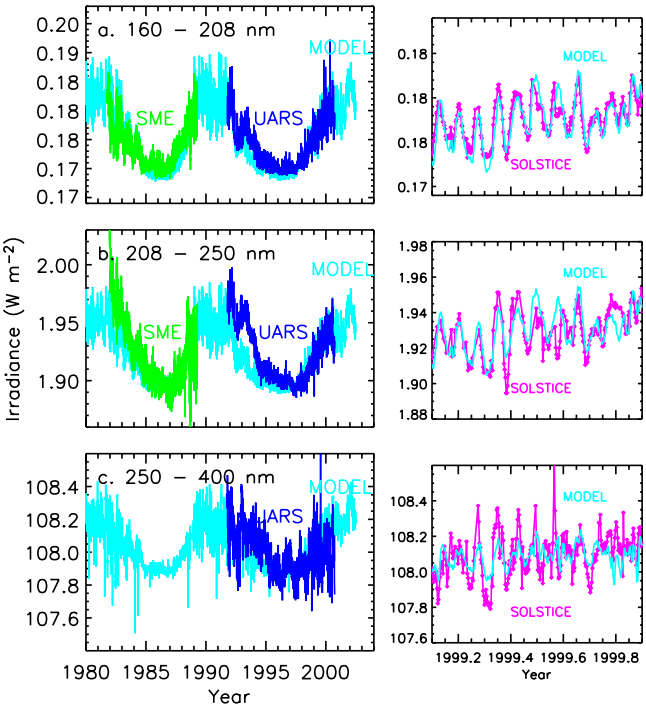

Fig. 27. Empirical models constructed from combinations of the facular brightening and sunspot darkening indices in Fig. 21 are compared with observations in three UV bands during the solar cycle, on the left, and solar rotation, on the right. In each case, the absolute levels of the various observations have been adjusted to match those of the model.

irradiance variability. This motivated the development of SORCE's new approach for measuring solar spectral irradiance longward of 300 nm by using a prism and miniature electrical-substitution radiometer, rather than a grating and photomultiplier [52].

Models of solar irradiance variability at wavelengths longer than 400 nm, for which adequate observational databases are lacking, also utilize the sunspot darkening and facular brightening indices in Fig. 22 but rely on theoretical calculation [132] to provide information about their relative roles, as quantified by the coefficients a_λ and b_λ. The wavelength dependencies of the contrasts of faculae and sunspots, shown in Fig. 23, determine appropriate combinations of P_S and P_F for reproducing irradiance variabilities at different wavelengths. This approach, described by Lean (2000), produced the estimates of solar cycle spectral irradiance variability at wavelengths longer than 400 nm, shown in Fig. 14. Future validation of spectral irradiance variability models at wavelength longward of 300 nm will be possible with SORCE observations. Initial results already suggest that model revisions are needed; in particular, the SORCE observations do not support facular contrasts as dark in the infrared spectrum as those shown in Fig. 23 [30].

6. Past and future irradiance variations

Knowledge of irradiance variations on much longer time scales than the few decades of direct observations are needed, for example to aid in the interpretation of past climate change. This knowledge must be inferred from indicators and proxy records of solar activity. The sunspot numbers since 1610, shown in Fig. 1, are the longest record of solar activity based on actual solar observations (see, e.g., [61]), and capture the Maunder Minimum epoch of anomalously low activity in the seventeenth century. Information extracted from observations of the terrestrial environment provide indirect evidence of solar activity. These proxies include the *aa* index of geomagnetic activity since 1882 [91] and the ^{14}C and ^{10}Be cosmogenic isotopes archived in tree-rings and ice-cores, respectively, over past millennia [11,13].

Reconstructing past solar irradiance from sunspot numbers, geomagnetic activity or cosmogenic isotopes is a challenging task. The most crucial aspect is establishing whether – or not – longer-term irradiance variability is present in addition to the known 11-year cycle. Long-term trends in the *aa* index and the cosmogenic isotopes, together with the range of variability in sun-like stars [8], suggest that the Sun is capable of a broader range of activity than witnessed during recent solar cycles. This implies the existence of one or more long-term irradiance variability components which models of historical irradiance have attempted to incorporate. But recent studies [48,51] refute the initial evidence from sun-like stars of a Maunder-Minimum-type behaviour as demonstrated by the bi-modal distribution of [8]. It seems that the lowest activity level of sun-like stars better corresponds to the brightness level of the minimum between the two distributions, rather than to the peak of the lower mode. Independent studies also raise the possibility of long-term instrumental drifts in the *aa* index [127], and question the assumption of a linear relationship between heliospheric-modulated proxies and solar irradiance [82].

6.1. Evidence for long-term solar activity changes

That solar activity evolves with time is evident in the sunspot group number, R_g, shown in Fig. 1. The amplitude of the 11-year activity cycle has varied by two orders of magnitude over the past 400 years, while the phase of the cycle has ranged from 8 to 15 years. Solar cycles with lower amplitudes tend to last longer, but the amplitude (Fig. 1b) and length (Fig. 1c) of solar cycles are only loosely related (correlation coefficient of -0.34). This suggests the behaviour of a non-linear oscillator (e.g., [94]) but the true origin of solar activity and the sunspot cycle is uncertain.

Waxing and waning sunspot numbers during the past four centuries, evident in Fig. 1, indicate fluctuations in solar activity that are undoubtedly accompanied by variations in many solar phenomena, including radiative output. When sunspot numbers are high, not only are there more, and larger, dark sunspots present on the Sun, but bright features (faculae, plages) are also larger and more frequent. High sunspot numbers correspond to increased gross magnetic flux (Fig. 19) and related solar indices, including the fluxes of the Ca, Mg and He chromospheric indices and the 10.7 cm radio emission (Fig. 8). Although the sunspot number is a numerical, rather than geophysical, proxy of solar activity, it tracks these indices rather closely: for example, the correlation coefficient

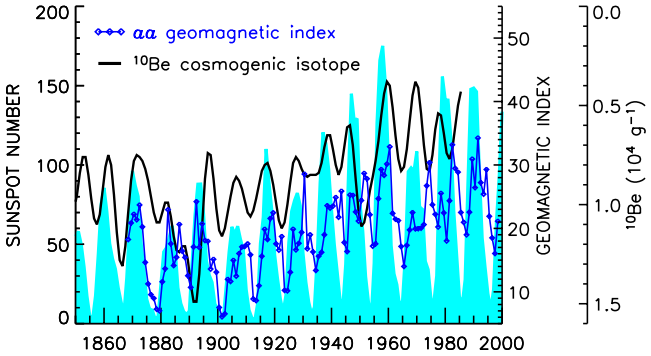

Fig. 28. Cosmogenic isotopes stored in tree-rings (^{14}C) and ice-cores (^{10}Be) provide indirect information about solar activity. The residence time of ^{10}Be in the climate system is sufficiently small that solar-induced changes are evident during the 11-year solar activity cycle (solid line), and are seen to track concurrent solar-induced changes in the *aa* index of geomagnetic activity (symbols) and sunspot numbers (shaded). In both the ^{10}Be and *aa* indices, the 11-year cycles are superimposed on a significant overall drift in the first half of the twentieth century that is not seen in sunspot numbers at solar minima

of daily sunspot numbers and 10.7 cm fluxes (shown in Fig. 8 since 1980) is 0.94 for daily non-zero values between 1947 and 2003. Hence, the combination of the number of groups g and the number of individual spots n, $R_z = 10g + n$, that Wolf devised for the definition of the Zürich sunspot number is more representative for solar activity in general than of spots per se [60, and references therein].

The *aa* geomagnetic index and the ^{10}Be cosmogenic isotope record likewise indicate the inconstancy of the Sun's 11-year activity cycle, as Fig. 28 illustrates during the past century. The *aa* index is recorded by magnetometers at antipodal locations on Earth (to mitigate the effect of the Earth's magnetic field) and it's variations reflect the impact of the solar wind (speed and density) and heliosphere (interplanetary magnetic field) on the magnetosphere [108,125]. The cosmogenic isotopes are the products of galactic cosmic ray interactions with gases in the Earth's atmosphere. Levels of cosmic ray fluxes are reduced during times of high solar activity because enhanced open flux from the Sun impedes their motion through the heliosphere and reduces the number that reaches the Earth. As with geomagnetic activity, cosmic ray fluxes reflect heliospheric variability, including the solar wind structure, strength of the interplanetary magnetic field, and the tilt angle of the heliospheric current sheet [15,104].

Cosmogenic isotopes are the primary proxy of solar activity prior to about 1600. As Fig. 29 shows, their anti-correlation with sunspot numbers, evident in Fig. 28 during the 11-year cycle, persists during the past millennium, including an increase in the Maunder Minimum and other similar solar activity minima [10,13]. Both the ^{14}C and ^{10}Be records exhibit common cycles that are apparently solar-related (reflecting that the Sun is the common source of their production) with periods near 90 years, called the Gleissberg cycle, and near 205 years, in addition to the 11-year cycle [97].

Attempts to reconstruct sunspot numbers prior to 1600 yield ambiguous results. The extrapolation of cycles identified by spectral decomposition of the sunspot record itself indicates solar activity in the Medieval Maximum (1140–1200) only slightly less than

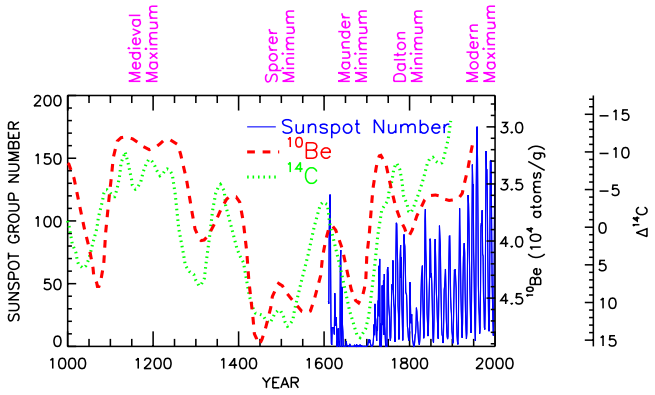

Fig. 29. Shown are the records of cosmogenic isotope fluctuations in tree-rings and ice-cores associated with solar activity during the past millennium. The long-term trends in the cosmogenic isotopes track the envelope of sunspot number amplitudes

in the present Modern Maximum (1900–2000) [109]. In contrast, an inversion of the ^{10}Be suggests that the Sun has been unusually active since the 1940s, relative to the past millennium [133, 134]. Both approaches agree, however, that sunspot numbers between 1400 and 1700 were reduced significantly relative to current levels as a consequence of the Spörer and Maunder minima (Fig. 29).

There are also conflicting interpretations of the various solar proxies in Figs. 28 and 29 in terms of long-term variations in solar magnetic flux. By analyzing the *aa* index to isolate the solar sources of its variability [89] infer a doubling of the Sun's coronal magnetic field strength since 1900, and a 40 % increase since 1964 (see also [86]). In contrast the last two cycles of solar magnetic field data show no secular trend in photospheric flux in the immediate past [6]. Furthermore, it is the open coronal flux, not the total flux, that extends into the heliosphere and controls geomagnetic activity and cosmic ray fluxes [6, 15, 135].

According to simulations of the transport and evolution of emerging bipolar magnetic regions on the Sun's surface (which are the sources of active regions and sunspots), and the spreading of magnetic flux into interplanetary space, secular trends in open magnetic flux need not necessarily infer equivalent secular trends in total magnetic flux, i.e., in solar activity [82, 135]. The simulations suggest that increasing solar cycle amplitudes, such as seen in sunspot number cycles from 1900 to 1950, can indeed cause an accumulation of open flux and a long-term secular trend, and hence cause a drift in cosmogenic isotopes and geomagnetic activity. However, the total magnetic flux (of which only 10 % extends into the heliosphere) does not exhibit a concurrent secular trend. Contrary claims, that ^{10}Be is a good proxy for the total surface magnetic fields, arise from studies that postulate ephemeral region sources of magnetic flux (parameterized by solar cycle length) in addition to the larger bipolar magnetic regions associated with active regions parameterized by sunspot numbers [122, 123].

Evidence for long-term changes in ephemeral regions is, however, uncertain. Although postulated to vary in a significant way on long-term scales from a comparison of current solar activity with the distribution of Ca brightness in sun-like stars [32, 139]

did not detect in Ca K solar images long-term changes in the network, where ephemeral regions mainly reside. And a reassessment of the stellar data has been unable to recover the original bimodal separation of (lower) Ca emission in non-cycling stars compared with (higher) emission in cycling stars [51]. In their interpretation of the original bimodal distribution from [8, 139] had inferred solar Ca K levels during the Maunder Minimum that matched the stellar Ca levels of the non-cycling stars at the peak of the lower bi-modal distribution. It is interesting to note that [139] found that a Sun with all the magnetic network removed from the present minima would lie approximately at the minimum between the two distribution, which is now thought to better indicate the lowest possible activity level that sun-like stars may reach [48,51]. Additional reduction in the basal emission from the centers of the network cells must be hypothesized in order to achieve the lower brightness levels of non-cycling stars [139].

Speculated long-term variability mechanisms in addition to changes in the area of ephemeral regions include fluctuations in facular brightness, in solar diameter [119] and in sub-surface convective strength [58].

6.2. The Maunder Minimum

Whereas many sunspots are present during contemporary solar maxima (e.g., 1980, 1990), they were less prevalent in the centuries before 1900. During the 17th-century Maunder Minimum, from 1645 to 1715, sunspots were absent from the disk entirely for long periods [26]. This is the only such episode of a spot-less Sun in the available sunspot record. A less severe and less prolonged episode of reduced solar activity, the Dalton Minimum, occurred near 1800 (Figs. 1, 29). During past millennia, series of Maunder-like solar activity minima punctuate the Sun's activity, as indicated by cosmogenic isotopes. The Spörer Minimum can be seen in Fig. 29 to immediately precede the Maunder Minimum; other similar minima are evident episodically during the past 10,000 year record of ^{14}C (e.g., around 800 BC).

Conceptually, the excess cosmogenic isotopes in the Maunder and other solar minima relative to the present is associated with reduced and less structured heliospheric magnetic fields. However, [136] suggest that with the reduced solar activity the modulation of the interplanetary magnetic field derived from the open flux associated with the very low sunspot numbers is too small to account for the significant fluctuations of ^{10}Be during the Maunder Minimum [14], including apparent cyclicity. Ephemeral regions are, once again, postulated, as an additional source of open flux to explain why ^{10}Be levels fluctuated during the seventeenth century [123].

An adequate physical understanding of the solar processes (from the interior dynamo to the extended heliosphere) that simultaneously altered cosmogenic isotopes and sunspot numbers during the Maunder Minimum remains to be achieved. There are also concerns about a possible climate influence on cosmogenic isotopes, which may compromise their fidelity as indicators of pure solar activity. Climate change affects the deposition of cosmogenic isotopes in their respective archives, and may contribute additional variations to that imposed by solar-induced production (e.g., [70,92]), especially during times of negligible manifestations of solar activity.

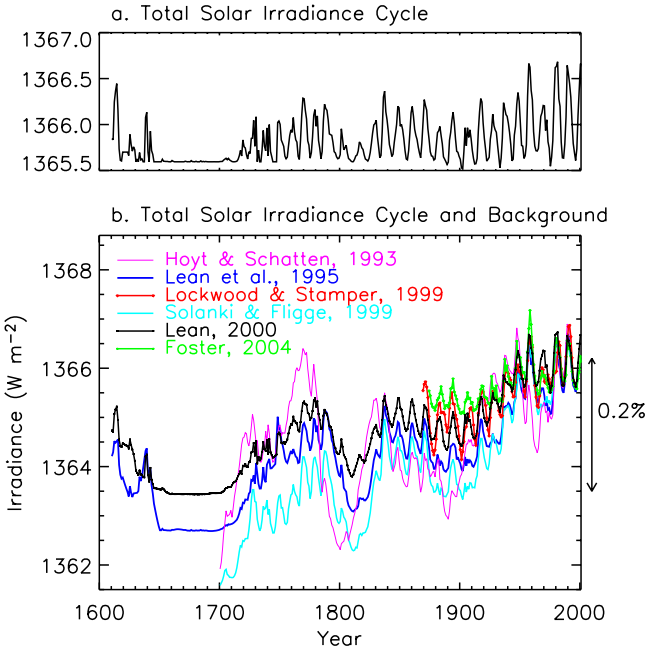

Fig. 30. Shown in **(a)** are variations in the total solar irradiance arising from changes in solar activity during the 11-year solar cycle. The time series is determined from the correlation of the annual means of observed total solar irradiance and sunspot numbers. The historical irradiance reconstructions shown in **(b)** all assume the existence of a longer term source of irradiance variability, in addition to the 11-year cycle. Their different long-term trends reflect different assumptions about the irradiance reduction during the Maunder Minimum relative to the present. For comparison, the absolute scales of the various reconstructions have been adjusted by constant offsets to agree during the contemporary epoch

6.3. Long-term irradiance reconstructions

Direct, instrumental measurements of solar irradiance from satellite measurements, although available for only the past 25 years, indicate that solar irradiance (Fig. 2) is increased when sunspot numbers (Fig. 8) are high. The direct correlation of annual mean total solar irradiance and sunspot number allows estimates of solar irradiance cycles directly from the long-term sunspot record in Fig. 1. Such a reconstruction is shown in the upper panel of Fig. 30, and indicates that contemporary irradiance cycles are the largest of the past 400 years. When reconstructed from a linear transformation of sunspot numbers, irradiance levels during the Maunder Minimum are estimated to be similar to those of current cycle minima [73, 118].

But high sunspot numbers actually correspond to increased sunspot darkening and increased facular brightening (Fig. 22), both of which alter solar irradiance, but in opposite ways. The approach of modelling contemporary total solar irradiance variations using sunspot and facular proxies has also been adopted for reconstructing longer term irradiance variations. Sunspot darkening is determined since the 1880s from Greenwich Observatory white light solar observations, and is assumed to be zero during the Maun-

der Minimum. Estimating a facular index prior to 1975 is, however, problematic. The irradiance reconstructions shown in Fig. 30b all postulate a source of long-term irradiance variability on multi-decadal to centennial time scales, based on circumstantial evidence from geomagnetic activity [88], cosmogenic isotopes [120], variations in sun-like stars [74, 75] and changes in interior solar structure implied by evolving sunspot umbral and penumbral ratios [58]. A facular index is then developed from, for example, the smoothed amplitude of the 11-year R_g cycle [74, 75, 120] or its instantaneous period (i.e., cycle length [58, 120]) with the amplitude scaled to match circumstantial evidence. As Fig. 1 shows, the temporal structure of these two quantities are rather different from each other. The most recent irradiance reconstructions utilize both the sunspot amplitude and the cycle length, to parameterize, the sunspot and active region irradiance sources, respectively, and the assumed ephemeral region changes [87, 121]. Lean et al. [77] estimated the level of irradiance during the Maunder Minimum to be 2.7 $\mathrm{W\,m^{-2}}$ below present minima, corresponding to non-cycling stars at the peak of the lower mode of the bi-modal distribution. As a result of a revised transfer of the stellar Ca HK to solar Ca K values by Lean [74] this reduction was determined to be 2.2 $\mathrm{W\,m^{-2}}$. They also estimated a reduction of 1.5 $\mathrm{W\,m^{-2}}$ for a non-magnetic Sun. This value was obtained from knowledge of the network contrast and fractional disk coverage in the contemporary Sun, and is independent of the brightness distribution of sun-like stars. It is interesting to note that it is very close to a recent determination from MDI/SOHO data by [31] of 1.7 ± 0.1 $\mathrm{W\,m^{-2}}$.

Which of the time series in Fig. 30 better represents actual irradiance variability is unknown. The primary uncertainty is whether the secular changes that the models assume actually occur [146], or not [32, 82]. Nor is the extant contemporary database of sufficient duration to adequately judge the various approaches. The comparisons in Fig. 31 show that the historical reconstructions deviate from each other prior to 1980, which is when actual observations were just commencing. Lack of a clear physical relationship between the ^{14}C and ^{10}Be cosmogenic isotopes and irradiance variability is a critical impediment to improved understanding of long-term irradiance variability. Whereas the sources of irradiance variability are magnetic active regions near the surface of the Sun, cosmogenic isotopes variations occur because the extended solar atmosphere in interplanetary space modulates the flux of galactic cosmic rays that reaches the Earth's atmosphere [10, 137]. The recent simulations of magnetic flux transport on the Sun, suggesting the lack of a linear relationship between total and open flux (and hence irradiance and the interplanetary magnetic field) are preliminary, and raise additional questions about the role or meridional transport and the extrapolation of surface magnetic fields to the corona and heliosphere that require further study. Even assuming secular irradiance changes to be present, most estimates of solar irradiance variability over the past thousand or so years indicate amplitude changes of 2 to 3 tenths of a percent on time scales of a few hundred years.

Like the solar cycle changes, long-term irradiance variations, if they exist, can be expected to have significant spectral dependence. The reconstructions of selected broad spectral bands shown in Fig. 32 present scenarios in which solar spectral irradiance is determined as $F(\lambda, t) \propto a_\lambda P_S(t) + b_\lambda P_F(t) + c_\lambda I_L(t)$ where I_L is the smoothed sunspot group number from Fig. 1, and c_λ accounts for the wavelength-dependent amplitude of the long-term component. The long-term component is scaled such that it produces an

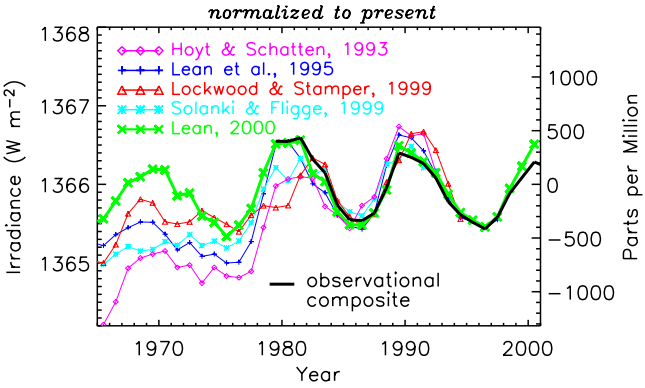

Fig. 31. The reconstructions of historical total solar irradiance shown in Fig. 30b are compared with annual means of the observational composite time series. It is important to note that this is a crucial test for the validity of a reconstruction: failure to reproduce the present three irradiance cycles indicates an incorrect parameterization of some sort

irradiance change from 1650 to 1986 approximately equal to the solar cycle variation in the facular component of the variability. Also shown, for comparison, are reconstructions of the 11-year activity cycle alone, i.e., with $c_\lambda = 0$.

6.4. Future irradiance scenarios

Levels of future solar activity cycles are routinely predicted using two techniques that estimate sunspot numbers and 10.7 cm fluxes. The statistical regression technique employs the sunspot record to quantify average properties and mean behaviour patterns [54]. The geophysical precursor technique recognizes the extended nature of the solar cycle and uses geophysical indices during descending and minima phases to predict subsequent maxima [128]. An alternative precursor approach invokes solar dynamo theory to forecast cycle maxima from the strength of the Sun's polar fields at minima [117]. Future levels of the Sun's irradiance corresponding to predicted cycles of the 10.7 cm flux, shown in Fig. 33, are estimated from a parameterization of annual total solar irradiance and 10.7 cm radio flux. The observational irradiance database is too short for the detection or understanding of long-term solar irradiance trends that may affect future solar radiative output but speculations are possible by assuming that historical irradiance reconstructions during the past 350 years (e.g., Fig. 30b) sample the plausible range. With this assumption, maximum total irradiance trends are $\pm 0.4\ \mathrm{W\,m^{-2}}$ per decade [78]. The dashed lines in Fig. 33 indicate these trend limits.

The fact that current levels of solar activity are at overall high levels, according to both the sunspot numbers and cosmogenic isotopes, may imply that future solar irradiance values will not be significantly higher than seen in the contemporary database. A projection of future solar activity based on spectral synthesis of the cosmogenic isotope record confirms that solar activity is presently peaking, and in 2100 will reach levels comparable to those in 1990 [18]. Projections of combined 11-, 88- and 208-year solar cycles also suggest that overall solar activity will increase in the near future, but only

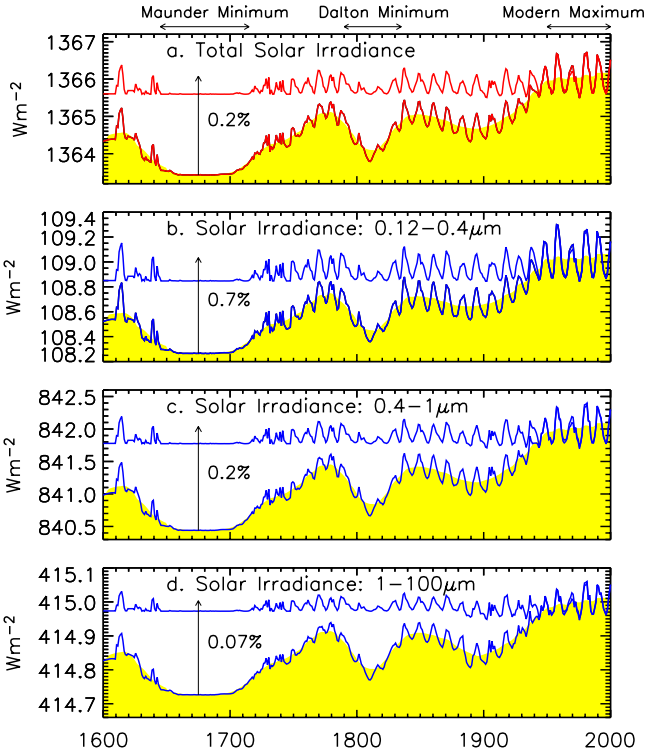

Fig. 32. Model estimates of long-term variability in the total solar irradiance and in three spectral bands in the UV, visible and IR. In these calculations, the adopted amplitude of the long-term facular component is approximately equal to its contemporary solar cycle amplitude. Reconstructions of 11-year cycles alone are also shown

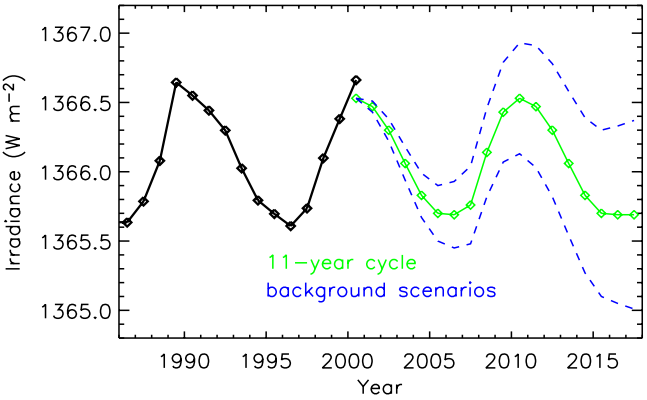

Fig. 33. Shown are projected total solar irradiance variations obtained from predictions of the 10.7 cm flux in future solar cycles made by [117]. The dashed lines indicate the range of plausible trends assuming the maximum rate of change of the [74] historical irradiance in Fig. 30

until 2030, followed by decreasing activity until 2090 [63]. In contrast, a numerical model of solar irradiance variability which combines cycles related to the fundamental 11 year cycle by powers of 2 predicts an irradiance decrease of 0.05 % during the next two decades [101]. A lack of physical understanding how dynamo-driven solar activity produces the competing effects of sunspot blocking and facular brightening, cautions against future predictions, even of 11-year cycle amplitudes.

7. Conclusions

Knowledge and understanding of solar radiative output and its variability has advanced rapidly in the space era. Crucial for this advance is the observational record of total solar irradiance (TSI), monitored continuously since late 1978 by electrically calibrated radiometers on several overlapping space missions. The observations provide definitive evidence that the Sun is about 0.1 % brighter during recent maxima than during minima of the 11-year activity cycles. Although the question of a contemporary long-term trend of TSI is still under discussion, there are strong arguments in support of constant radiative output levels during the last two solar activity minima. Knowledge and understanding of the spectral irradiance variations that compose the total are far less certain, primarily because of the lack of sufficient long-term observations with the needed accuracy and spectral coverage. While irradiance variability is relatively well known at wavelengths below about 300 nm, where it exceeds that of TSI by large factors (up to orders of magnitude), concomitant advances in understanding of the variations in most of the spectrum await new measurements such as those recently commenced by next-generation instrumentation on the SORCE spacecraft. Initial results demonstrate unequivocally the variability of solar spectral irradiance at all wavelengths, not just in the UV spectrum.

Clearly evident in the more than 25-year long record of daily values of a composite TSI record, constructed from the individual observations, are the prominent roles of dark sunspots and bright faculae (in active regions and the surrounding network) as sources of irradiance variability. Empirical models confirm this understanding; combining the sunspot darkening index, P_S, and P_F, an index for the brightening due to faculae and network (such as the Mg II index), accounts for nearly 80 % of the observed variance of total solar irradiance during the 11-year solar activity cycle. Allowing for the wavelength dependence of the contrasts of sunspots and faculae provides a first order description of spectral irradiance variations, currently limited by poor knowledge of facular contrasts especially in the near infrared spectrum. The empirical models support the zero-trend hypothesis of contemporary irradiance, thereby constraining mechanisms of such a trend, should they exist, to other than those magnetic features responsible for the 11-year irradiance cycle.

Because relationships between solar irradiance and solar activity are, thus far, largely empirical, their implications for long-term variability are uncertain. Robust understanding of solar irradiance variability ultimately requires that the various solar activity indices and proxies be physically derived from solar magnetic fields. On longer time-scales, possible mechanisms must be validated and detected in the instrumental record, separately from non-solar influence. A dynamo at the base of the convection zone governs the emergence, reorganization and transport of magnetic activity that produces the waxing and waning of surface magnetic fields, and the resultant dark sunspots, bright faculae

and network that modulate solar irradiance. Thus, a complete physical specification of irradiance variations involves processes below the solar surface as well as in the solar atmosphere.

Rapid progress in understanding the interior of the Sun also occurred during the space era as a result of helioseismology and its impact on major improvements of the standard solar model, such as more accurate opacities and a better equation of state. But the physical understanding and characterization of structures in the solar atmosphere, from the photosphere out to the corona, and their impacts on radiative outputs, is less advanced. Radiative transfer calculations which formulate our understanding of radiative output in the direction of the Earth – that is, the irradiance – are based on temperature distributions with height which match the observations. Self-consistent theoretical calculations are still not possible mainly due to the lacking understanding of the details of the energy transport.

Knowledge of solar irradiance variability prior to the space era is rudimentary, as demonstrated by the range of values for total solar irradiance prescribed for the seventeenth century Maunder Minimum. Postulating an irradiance reduction below that of contemporary solar minima requires the identification of mechanisms in addition to the sunspot and faculae fluctuations that produce the 11-year cycle. One scenario is the removal of the bright faculae that compose the "quiet" network surrounding supergranular cells, even in contemporary solar minimum. Such a removal is estimated to reduce total solar irradiance by about 1.5 $\mathrm{W\,m^{-2}}$, or slightly more than 0.1 % below current solar minimum levels. Larger-amplitude irradiance reductions require additional mechanisms, such as the overall dimming of the basal emission from cell centers, or changes in radius or interior structure. However, quantitative knowledge of such speculated mechanisms is lacking. Inferences made from long-term trends in cosmogenic isotope proxies suffer from the inability, thus far, to quantify the physical relationships between closed magnetic flux that relates to irradiance, versus the open flux that pervades the heliosphere and modulates the galactic cosmic rays that produce the cosmogenic solar activity proxies. Determining whether – or not – and why, solar irradiance varies on long time scales will require considerable additional research and understanding, and much longer irradiance time series.

Acknowledgements. Continued support of solar irradiance research at PMOD/WRC by the Swiss National Science Foundation is greatly acknowledged, including support of C. Fröhlich's contributions to this review. NASA and The Office of Naval Research supported the contributions of J. Lean (including NASA UARS, LWS and SORCE grants). Very much appreciated are the efforts of the many observers and instrumentalists who produced the data sources that this review utilizes, and the NOAA NGDC which archives many of the datasets. Included are unpublished data from VIRGO on SOHO, a cooperative ESA/NASA mission and from ACRIM III on ACRIM-Sat. During the preparation of this review, C. Fröhlich and J. Lean have benefited from many helpful discussions with the solar irradiance community, including R. B. Lee, R. C. Willson, G. J. Rottman and O. R. White.

References

1. C.G. Abbot: *Smithsonian Misc.Coll.* 117, 1 (1952)
2. C.G. Abbot: *Smithsonian Misc.Coll.* 146, 1 (1963)
3. L.B. Aldrich, W.H. Hoover: *Annals of the Astrophysical Observatory of the Smithsonian Institution*, vol. 7, chap.7: Statistical Studies of the Solar-Constant Record, pp. 165–168. Smithsonian Institution, Washington, DC, USA (1954)
4. C.W. Allen: *Astrophysical Quantities*. Athlone, London, 3rd edn (1981)
5. H.M. Antia, S. Basu, F. Hill, R. Howe, R.W. Komm, J. Schou: *MNRAS* 327, 1029 (2001)
6. C.N. Arge, E. Hildner, V.J. Pizzo, J.W. Harvey: *J. Geophys. Res.* 107, 1319 (2002)
7. E.H. Avrett: Modelling solar variability – synthetic models. In: J. Pap, C. Fröhlich, R. Ulrich (eds) *Proceedings of the SOLERS22 Workshop, Sacramento Peak, June 1996*, pp. 449–469. Kluwer, Dordrecht, The Netherlands (1998)
8. S. Baliunas, R. Jastrow: *Nature* 348, 520 (1990)
9. N.J. Balmforth, D.O. Gough, W.J. Merryfield: *MNRAS* 278, 437 (1996)
10. E. Bard, G. Raisbeck, P. Yiou, J. Jouzel: *Tellus B* 52, 985 (2000)
11. E. Bard, G.M. Raisbeck, F. Yiou, J. Jouzel: *Earth and Planetary Science Letters* 150, 453 (1997)
12. S. Basu: What does helioseismology tell us about solar cycle related structural changes in the sun? In: A. Wilson (ed.) *SOHO-11: From Solar Minimum to Maximum*, pp. 7–14. SP-508, ESA Publ. Division, ESTEC, Norrdwijk, The Netherlands (2002)
13. J. Beer: *Space Sci. Rev.* 94, 53 (2000)
14. J. Beer, S.M. Tobias, N.O. Weiss: *Sol. Phys.* 181, 237 (1998)
15. H.V. Cane, G. Wibberenz, I.G. Richardson, T.T. von Rosenvinge: *Geophys. Res. Lett.* 26, 565 (1999)
16. W.J. Chaplin, Y. Elsworth, G.R. Isaak, B.A. Miller, R. New: *MNRAS* **352**, 1102 (2004)
17. G.A. Chapman, A.M. Cookson, J.J. Dobias: *J. Geophys. Res.* 101, 13541 (1996)
18. M.A. Clilverd, E. Clarke, H. Rishbeth, T.D. G. Clark, T. Ulich: *Astronomy and Geophysics* 44, 20 (2003)
19. D. Crommelynck, V. Domingo, A. Fichot, C. Fröhlich, B. Penelle, J. Romero, Ch. Wehrli: *Metrologia* 30, 375 (1993)
20. D. Crommelynck, A. Fichot, R.B. Lee III, J. Romero: *Adv. Space Res.* 16, 17 (1995)
21. T.J. Crowley: *Science* 289, 270 (2000)
22. U. Cubasch, R. Voss: *Space Sci. Rev.* 94, 185 (2000)
23. G. de Toma, O.R. White, B.G. Knapp, G.J. Rottman, T.N. Woods: Mg II core-to-wing index: Comparison of SBUV2 and SOLSTICE time series. *J. Geophys. Res.* 102, 2597 (1997)
24. A.E. Dessler, M.D. Burrage, J.-U. Grooss, J.R. Holton, J.L. Lean, S.T. Massie, M.R. Schoeberl, A.R. Douglass, C.H. Jackman: *Reviews of Geophysics* 36, 183 (1998)
25. M. Dikpati, P. Charbonneau: *ApJ* 518, 508 (1999)
26. J.A. Eddy: *Science* 192, 1189 (1976)
27. M. Fligge, S.K. Solanki: *Sol. Phys.* 173, 427 (1997)
28. M. Fligge, S.K. Solanki: *Geophys. Res. Lett.* 27, 2157 (2000)
29. J. Fontenla, O.R. White, P.A. Fox, E.H. Avrett, R.L. Kurucz: *ApJ* 518, 480 (1999)
30. J.M. Fontenla, J. Harder, G. Rottman, T. Woods, G.M. Lawrence, S. Davis: *ApJ* 605, L85 (2004)
31. S.S. Foster: *Reconstruction of Solar Irradiance Variations for use in Studies of Global Climate Change: Application of Recent SOHO Observations with Historic Data from the Greenwich Observatory*. PhD thesis, University of Southhampton, Faculty of Science, School of Pysics and Astronomy (2004)
32. P. Foukal L. Milano: *Geophys. Res. Lett.* 28, 883 (2001)
33. P. Foukal, J. Vernazza: *ApJ* 234, 707 (1979)

34. P.V. Foukal, J. Lean: *ApJ* 302, 826 (1986)
35. P.V. Foukal, J. Lean: *ApJ* 328, 347 (1988)
36. P.V. Foukal, P.E. Mack, J.E. Vernazza: *ApJ* 215, 952 (1977)
37. C. Fröhlich: Contemporary measures of the solar constant. In: O.R. White (ed.) *The Solar Output and its Variation*, pp. 93–109 (1977)
38. C. Fröhlich: *Space Sci. Rev.* 94, 15 (2000)
39. C. Fröhlich: *Metrologia* 40, 60 (2003)
40. C. Fröhlich: Solar Irradiance Variations. In: *Proc. ISCS 2003: Solar Variability as an Input to the Earth's Environment*. SP-535, ESA Publ. Division, ESTEC, Norrdwijk, The Netherlands (2003)
41. C. Fröhlich: Solar Irradiance Variability. In: *Geophysical Monograph 141: Solar Variability and its Effect on Climate*, chap. 2: Solar Energy Flux Variations, pp. 97–110. American Geophysical Union, Washington DC, USA (2004)
42. C. Fröhlich, B. Andersen, T. Appourchaux, G. Berthomieu, D.A. Crommelynck, V. Domingo, A. Fichot, W. Finsterle, M.F. Gómez, D.O. Gough, A. Jiménez, T. Leifsen, M. Lombaerts, J.M. Pap, J. Provost, T. Roca Cortés, J. Romero, H. Roth, T. Sekii, U. Telljohann, T. Toutain, C. Wehrli: *Sol. Phys.* 170, 1 (1997)
43. C. Fröhlich, D. Crommelynck, C. Wehrli, M. Anklin, S. Dewitte, A. Fichot, W. Finsterle, A. Jiménez, A. Chevalier, H.J. Roth: *Sol. Phys.* 175, 267 (1997)
44. C. Fröhlich, J. Lean: *Geophys. Res. Lett.* 25, 4380 (1998)
45. C. Fröhlich, J. Lean: Total solar irradiance variations: The construction of a composite and its comparison with models. In: F.L. Deubner, J. Christensen-Dalsgaard, D. Kurtz, (eds) *IAU Symposium 185: New Eyes to See Inside the Sun and Stars*, pp. 89–102. Kluwer, Dordrecht, The Netherlands (1998)
46. C. Fröhlich, J. Lean: *Astron. Nachr.* 323, 203 (2002)
47. M.A. Geller, S.P. Smyshlyaev: *Geophys. Res. Lett.* 29, 2048 (2002)
48. M.S. Giampapa, J.C. Hall, R.R. Radick, S.L. Baliunas: *AAS/Solar Physics Division Meeting* 34 (2003)
49. D.F. Gray, W.C. Livingston: *ApJ* 474, 802 (1997)
50. J.D. Haigh: *Phil. Trans. Roy. Soc. A* 361, 95 (2003)
51. J.C. Hall, G.W. Lockwood: *American Astronomical Society Meeting* 204 (2004) Abstract 03.02
52. J. Harder, G.M. Lawrence, G. Rottman, T. Woods: *Metrologia* 37, 415 (2000)
53. K.L. Harvey, O.R. White: *Astron. Soc. Pacific Conf. Ser.* 140, 247 (1998)
54. D.H. Hathaway, R.M. Wilson, E.J. Reichmann: *J. Geophys. Res.* 104. 22375 (1999)
55. D.F. Heath, M.P. Thekaekara: The solar spectrum between 1200 and 3000 Å. In O.R. White, editor, *The Solar Output and its Variation*, pp. 193 (1977)
56. R. Howe, J. Christensen-Dalsgaard, F. Hill, R.W. Komm, R.M. Larsen, J. Schou, M.J. Thompson, J. Toomre: *Science* 287, 2456 (2000)
57. D.V. Hoyt, H.L. Kyle, J.R. Hickey, R.H. Maschhoff: *J. Geophys. Res.* 97, 51 (1992)
58. D.V. Hoyt, K.H. Schatten: *J. Geophys. Res.* 98, 18895 (1993)
59. D.V. Hoyt, K.H. Schatten: *The Role of the Sun in Climate Change*. Oxford University Press, Oxford GB (1997)
60. D.V. Hoyt, K.H. Schatten: *Sol. Phys.* 181, 491 (1998)
61. D.V. Hoyt, K.H. Schatten, E. Nesme-Ribes: *Geophys. Res. Lett.* 21, 2067 (1994)
62. K. Hufbauer: *Exploring the Sun*. The Johns Hopkins University Press, Baltimore (1991)
63. J.L. Jirikowic, P.E. Damon: *Climatic Change* 26, 309 (1994)
64. L.H. Koopmans: *The Spectral Analysis of Time Series*. Academic Press, London, GB (1974)
65. G.A. Kopp, G. Lawrence, G. Rottman: What is the Accuracy of the Total Irradiance Monitor? *AGU Fall Meeting Abstracts* (2003) Abstract SH31C-C7
66. N.A. Krivova, S.K. Solanki, M. Fligge, Y.C. Unruh: *A&A* 399, L1 (2003)

67. J.R. Kuhn, K.G. Libbrecht: *ApJ* 381, L35 (1991)
68. R.L. Kurucz: New opacity calculations. In: L. Crivellari, I. Hubeny, D.G. Hummer (eds) *Stellar Atmospheres: Beyond Classical Models*, pp. 441–448. NATO ASI Ser. C 341, Kluwer, Dordrecht, The Netherlands (1991)
69. R.L. Kurucz: The solar spectrum. In: A.N. Cox, W.C. Livingston, M.S. Matthews (eds) *Solar interior and atmosphere*, pp. 663–669. University of Arizona Press, Tucson, AZ, USA (1991)
70. D. Lal: *Geophys. Res. Lett.* 14, 785 (1987)
71. G.M. Lawrence, G. Rottman, J. Harder, T. Woods: *Metrologia*, 37, 407 (2000)
72. J.K. Lawrence, G.A. Chapman, A.D. Herzog: *ApJ* 324, 1184 (1988)
73. J. Lean: *ARA&A* 35, 33 (1997)
74. J. Lean: *Geophys. Res. Lett.* 27, 2425 (2000)
75. J. Lean, J. Beer, R. Bradley: *Geophys. Res. Lett.* 22, 3195 (1995)
76. J. Lean, D. Rind: *Science* 292, 234 (2001)
77. J. Lean, A. Skumanich, O. White: *Geophys. Res. Lett.* 19, 1595 (1992)
78. J.L. Lean: *Geophys. Res. Lett.* 28, 4119 (2001)
79. J.L. Lean, J. Cook, W. Marquette, A. Johannesson: *ApJ* 492, 390 (1998)
80. J.L. Lean, T.P. Repoff: *J. Geophys. Res.* 92, 5555 (1987)
81. J.L. Lean, G.J. Rottman, H.L. Kyle, T.N. Woods, J.R. Hickey, L.C. Puga: *J. Geophys. Res.* 102, 29939 (1997)
82. J.L. Lean, Y.-M. Wang, N.R. Sheeley: *Geophys. Res. Lett.* 29, 2224 (2002)
83. J.L. Lean, O.R. White, W.C. Livingston, J.M. Picone: *J. Geophys. Res.* 106, 10645 (2001)
84. R.B. Lee III, B.R. Barkstrom, R.D. Cess: *Appl. Opt.* 26, 3090 (1987)
85. R.B. Lee III, M.A. Gibson, R.S. Wilson, S. Thomas: *J. Geophys. Res.* 100, 1667 (1995)
86. M. Lockwood: *J. Geophys. Res.* 106, 16021 (2001)
87. M. Lockwood: Solar outputs, their variations and their effects on earth. In: M. Güdel, I. Rüedi, W. Schmutz (eds) *Saas-Fee Advanced Courses, Number 32: The Sun, Solar Analogs and the Climate*. Springer-Verlag, Heidelberg, Germany (2004) (in press)
88. M. Lockwood, R. Stamper: *Geophys. Res. Lett.* 26, 2461 (1999)
89. M. Lockwood, R. Stamper, M.N. Wild: *Nature* 399, 437 (1999)
90. P. Maltby, E.H. Avrett, M. Carlsson, O. Kjeldseth-Moe, R.L. Kurucz, R. Loeser: *ApJ* 306, 284 (1986)
91. P.N. Mayaud: *J. Geophys. Res.* 77, 6870 (1972)
92. K.G. McCracken: *J. Geophys. Res.* 109, A04101 (2004)
93. G.A. Meehl, W.M. Washington, T.M. L. Wigley, J.M. Arblaster, A. Dai: *Journal of Climate* 16, 426 (2003)
94. P.D. Mininni, D.O. Gomez, G.B. Mindlin: *Sol. Phys.* 208, 167 (2002)
95. T. Moran, P. Foukal, D. Rabin: *Sol. Phys.* 142, 35 (1992)
96. R.W. Noyes, J.C. Raymond, J.G. Doyle, A.E. Kingston: *ApJ* 297, 805 (1985)
97. M.G. Ogurtsov, Y.A. Nagovitsyn, G.E. Kocharov, H. Jungner: *Sol. Phys.* 211, 371 (2002)
98. A. Ortiz, S.K. Solanki, V. Domingo, M. Fligge, B. Sanahuja: *A&A* 388, 1036 (2002)
99. A. Ortiz Carbonell: *Solar Irradiance Variations Induced by Faculae and small Magnetic Elements in the Photosphere*. PhD thesis, Unversitat de Barcelona, Departament d'Astronomia i Metrologia (2003)
100. J.P. Peixoto, A.H. Oort: *Physics of Climate*. American Institute of Physics (AIP), New York (1992)
101. C.A. Perry, K.J. Hsu: *PNAS* 97, 12433 (2000)
102. J.A. Plamondon: *JPL Space Prog. Summary* 37–59, 162 (1969)
103. J.A. Plamondon, J.M. Kendall, Sr.: *JPL Space Prog. Summary* 37-35, 66 (1965)
104. M.S. Potgieter, R.A. Burger, S.E.S. Ferreira: *Space Science Reviews* 97, 295 (2001)
105. J. Provost, G. Berthomieu, Morel P.: *A&A* 353, 775 (2000)

106. T.J. Quinn, C. Fröhlich: *Nature* 401, 841 (1999)
107. E. Ribes, B. Beardsley, T.M. Brown, P. Delache, F. Laclare, J.R. Kuhn, N.V. Leister: The variability of the solar diameter. In: C. Sonnet, M.S. Giampapa, and M.S. Matthews (eds) *Sun in Time*, pp. 59–97 (1991)
108. I.G. Richardson, E.W. Cliver, H.V. Cane: *J. Geophys. Res.* 105(A8), 18203 (2000)
109. N.R. Rigozo, E. Echer, L.E. A. Vieira, D.J. R. Nordemann: *Sol. Phys.* 203, 179 (2001)
110. D. Rind: *Science* 296, 673 (2002)
111. D. Rind, J. Lean, R. Healy: *J. Geophys. Res.* 104, 1973 (1999)
112. D. Rind, D. Shindell, J. Perlwitz, J. Lerner, P. Lonergan, J. Lean, C. McLinden: *Journal of Climate* 17, 906 (2004)
113. G. Rottman: *Space Sci. Rev.* 94, 83 (2000)
114. G. Rottman, G. Mount, G. Lawrence, T. Woods, J. Harder, S. Tournois: *Metrologia* 35, 707 (1998)
115. G. Rottman, L. Floyd, R. Viereck: Measurement of the Solar Ultraviolet Irradiance. In: J.M. Pap, P. Fox (eds) *Geophysical Monograph 141: Solar Variability and its Effect on Climate*, chapter 2: Solar Energy Flux Variations, pp. 111–126. American Geophysical Union, Washington DC, USA (2004)
116. I.-J. Sackmann, A.I. Boothroyd: *ApJ* 583, 1024 (2003)
117. K. Schatten, D.J. Myers, S. Sofia: *Geophys. Res. Lett.* 23, 605 (1996)
118. K.H. Schatten, J.A. Orosz: A solar constant model for sun-climate studies: 1600-2000AD. In: *Climate Impact of Solar Variability*, pp. 175–180 (1990)
119. S. Sofia, P. Fox: *Climate Change* 30, 1 (1994)
120. S.K. Solanki, M. Fligge: *Geophys. Res. Lett.* 26, 2465 (1999)
121. S.K. Solanki, N.A. Krivova, M. Schüssler, M. Fligge: *A&A* 396, 1029 (2002)
122. S.K. Solanki, M. Schüssler, M. Fligge: *Nature* 408, 445 (2000)
123. S.K. Solanki, M. Schüssler, M. Fligge: *A&A* 383: 706 (2002)
124. S.K. Solanki, Y.C. Unruh: *A&A* 329, 747 (1998)
125. R. Stamper, M. Lockwood, M.N. Wild, T.D. G. Clark: *J. Geophys. Res.* 104, 28325 (1999)
126. P.A. Stott, S.F. B. Tett, G.S. Jones, M.R. Allen, J.F. B. Mitchell, G.J. Jenkins: *Science* 290, 2133 (2000)
127. L. Svalgaard, E.W. Cliver, P. Le Sager: *Advances in Space Research* 34, 436 (2004)
128. R.J. Thompson: *Sol. Phys.* 148, 383 (1993)
129. G. Thuillier M. Meissonnier: Picard Mission. In: *SF2A-2002: Semaine de l'Astrophysique Francaise* (2002)
130. S. Turck-Chièze, S. Couvidat, A.G. Kosovichev, A.H. Gabriel, G. Berthomieu, A.S. Brun, J. Christensen-Dalsgaard, R.A. García, D.O. Gough, J. Provost, T. Roca-Cortes, I.W. Roxburgh, R.K. Ulrich: *ApJ* 555, L69 (2001)
131. Y.C. Unruh, S.K. Solanki, M. Fligge. *A&A* 345, 635 (1999)
132. Y.C. Unruh, S.K. Solanki, M. Fligge: *Space Sci. Rev.* 94, 145 (2000)
133. I.G. Usoskin, K. Mursula, S. Solanki, M. Schüssler, K. Alanko: *A&A* 413, 745 (2004)
134. I.G. Usoskin, S.K. Solanki, M. Schüssler, K. Mursula, K. Alanko: *Physical Review Letters* 91, 211101 (2003)
135. Y.-M. Wang, J. Lean, N.R. Sheeley: *Geophys. Res. Lett.* 27, 505 (2000)
136. Y.-M. Wang, N.R. Sheeley: *ApJ* 591, 1248 (2003)
137. W.R. Webber, P.R. Higbie: *J. Geophys. Res.* 108, (2003)
138. O.R. White, W.C. Livingston, S.L. Keil: *Astro. Soc. Pac. Conf. Ser.* 140, 293 (1998)
139. O.R. White, A. Skumanich, J. Lean, W.C. Livingston, S.L. Keil: *Publications of the Astronomical Society of the Pacific* 104, 1139 (1992)
140. R.C. Willson: *Space Sci. Rev.* 38, 203 (1984)
141. R.C. Willson: Irradiance observations from SMM, UARS and ATLAS experiments. In: J. Pap, C. Fröhlich, H.S. Hudson, and S. Solanki (eds) *The Sun as a Variable Star, Solar and Stellar Irradiance Variations*, pp. 54–62 (1994)

142. R.C. Willson: *Science* 277, 1963 (1997)
143. R.C. Willson: ACRIM II and ACRIM III data products (version 10/10/01). http://www.acrim.com/ in the directory Data%20Products.htm (2001)
144. R.C. Willson, S. Gulkis, M. Janssen, H.S. Hudson, G.A. Chapman: *Science* 211, 700 (1981)
145. R.C. Willson, H.S. Hudson: *Nature* 351, 42 (1991)
146. R.C. Willson, A.V. Mordvinov: *Geophys. Res. Lett.* 30, 1199 (2003)
147. T.N. Woods, F.G. Eparvier, J. Fontenla, J. Harder, G. Kopp, W.E. McClintock, G. Rottman, B. Smiley, M. Snow: *Geophys. Res. Lett.* 31, L10802 (2004)
148. T.N. Woods, D.K. Prinz, G.J. Rottman, J. London, P.C. Crane, R.P. Cebula, E. Hilsenrath, G.E. Brueckner, M.D. Andrews, O.R. White, M.E. Vanhoosier, L.E. Floyd, L.C. Herring, B.G. Knapp, C.K. Pankratz, et al.: *J. Geophys. Res.* 101, 9541 (1996)
149. J.R. Worden, O.R. White, T.N. Woods: *ApJ* 496, 998 (1998)